recently, Haze *et al.* (6) analyzed the body odor components that adhered to the shirts of the subjects by gas chromatography/mass spectrometry and demonstrated that 2-nonenal is present in increasing amounts in the body odors of persons 40 years or older. They have also suggested that *cis*-2-nonenal and *trans*-2-nonenal are formed from the oxidative degradation of polyunsaturated fatty acids, such as palmitoleic acid. However, it is still not clear how 2-nonenal could be formed *in vivo*. Because of its insolubility in water, 2-nonenal is less reactive with proteins than other 2-alkenals, such as acrolein and crotonaldehyde, and therefore has received relatively little attention as a causative agent for modification of proteins. Only inhibition of enzymes, such as platelet membrane-bound phosphotyrosine phosphatase (7) and liver microsomal glucose-6-phosphatase (8), has been reported.

A structurally diverse protein supergroup called scavenger receptors mediates the cellular uptake of modified lipoproteins. Scavenger receptors are expressed by endothelial cells, macrophages, and smooth muscle cells and mediate recognition, internalization, and physiological responses to a wide range of ligands, including phospholipids, lipoprotein particles, apoptotic cells, and pathogens. Several oxidized low density lipoprotein (LDL) receptors have been identified so far, including SR-A I/II, CD36, SR-BI, FcγRII, lectin-like oxidized LDL receptor (LOX-1), macrosialin, SR expressed by endothelial cells, etc. Among them, LOX-1 is characterized as the major receptor for oxidized LDL in the endothelial cells of large arteries. Its inducible expression (9) might be involved in the oxidized LDL-mediated endothelial dysfunction. LOX-1 exhibits a binding activity for multiple ligands. LOX-1 is capable of interacting with a variety of structurally and functionally distinct ligands, including oxidized LDL, platelets, aged red blood cells, apoptotic cells, advanced glycation end products, heat shock protein 70, bacteria, and phosphatidylserine (10). LOX-1 binds and internalizes a diverse array of macromolecules, although their structures are not always related to each other.

In this study, to understand the mechanism underlying the formation of a covalently modified protein with 2-nonenal *in vivo*, we raised a monoclonal antibody (mAb) against protein-bound 2-nonenal and identified a novel 2-nonenal-lysine adduct as the epitope. Our immunohistochemical studies demonstrated the localization of the immunoreactive materials in the kidney of rats exposed to Fe^{3+}-NTA, an iron chelate that induces acute renal proximal tubular necrosis, a consequence of free radical-mediated oxidative tissue damage, eventually leading to a high incidence of renal adenocarcinoma in rodents. Importantly, using high performance liquid chromatography with on-line electrospray ionization tandem mass spectrometry (LC/ESI/MS/MS), we also showed evidence that the 2-nonenal-lysine adduct is indeed accumulated during the lipid peroxidation-mediated modification of protein *in vitro* and *in vivo*. Furthermore, to evaluate the biological implication of the 2-nonenal modification of protein, we examined the involvement of LOX-1, a member of the scavenger receptor family, in the recognition of the 2-nonenal-lysine adducts.

EXPERIMENTAL PROCEDURES

Materials—*trans*-2-Nonenal (2-nonenal), N^{α}-acetyl-L-lysine, and human serum albumin (HSA) were obtained from the Sigma. Acrolein was obtained from Tokyokasei (Tokyo, Japan). N^{α}-[U-$^{13}C_6$,$^{15}N_2$]Fmoc-N^{ϵ}-boc-lysine (where boc is *t*-butoxycarbonyl) was obtained from the Cambridge Isotope Laboratories (Andover, MA). The keyhole limpet hemocyanin (KLH) was obtained from Pierce. Ferric nitrate nonahydrate, sodium carbonate, and bovine serum albumin (BSA) were from Wako (Osaka, Japan), and the nitrilotriacetic acid disodium salt was from Nacalai Tesque, Inc. (Kyoto, Japan). The Fe^{3+}-NTA solution was prepared immediately before use by the method described in a previous study (11). The stock solutions of 4-hydroxy-2-nonenal were prepared by the acid treatment (1 mM HCl) of 4-hydroxy-2-nonenal dimethyl acetal, which was synthesized according to the procedure of De Montarby *et al.* (12). 4-Oxo-2-nonenal was synthesized by the oxidation of 4-hydroxy-2-nonenal dimethyl acetal with pyridinium dichlorochromate, followed by HCl hydrolysis (13). The sodium salt of malondialdehyde was prepared by the Dowex hydrolysis of malondialdehyde bis(diethyl acetal) (14). Other aldehydes were purchased from Wako.

In Vitro Modification of HSA—Modification of the protein by 2-nonenal and its related short-chain aldehydes was performed by incubating HSA (1.0 mg/ml) with 0–10 mM 2-nonenal in 1 ml of 50 mM sodium phosphate buffer, pH 7.2, at 37 °C for 24 h. The Fe^{2+}-catalyzed oxidation of unsaturated fatty acids in the presence of HSA was performed by incubating HSA (1 mg/ml) with 2 mM unsaturated fatty acids in the presence of 50 μM Fe^{2+} and 1 mM ascorbic acid in 1 ml of 50 mM sodium phosphate buffer, pH 7.2, in atmospheric oxygen at 37 °C. The reaction was terminated by the addition of 1 mM butylated hydroxytoluene and 100 μM diethylenetriaminepentaacetic acid.

In Vitro Peroxidation of LDL—LDL (1.019–1.063 g/ml) was prepared from the plasma of healthy humans by sequential ultracentrifugation and then extensively dialyzed three times against phosphate-buffered saline (PBS, 10 mM sodium phosphate buffer, pH 7.2, containing 150 mM NaCl) containing 0.01% EDTA at 4 °C. LDL used for the oxidative modification by Cu^{2+} was dialyzed five times against a 1000-fold volume of PBS at 4 °C. The oxidation of LDL was performed by incubating 0.5 mg of LDL with $CuSO_4$ (5 μM) in 1 ml of PBS for 24 h at 37 °C. The reaction was terminated by the addition of 1 mM EDTA and then stored at 4 °C.

Amino Acid Analysis—An aliquot (0.2 ml) of the protein samples (1 mg/ml) incubated for 24 h at 37 °C in the absence or presence of 2-nonenal was treated with 10 mM EDTA (20 μl), 1 N NaOH (20 μl), and 100 mM sodium borohydride (20 μl). After incubation for 1 h at room temperature, 20 μl of 2 N HCl was added to the mixture to stop the reaction, and the mixture was then incubated for 60 min at room temperature after adding 280 μl of 20% trichloroacetic acid. After centrifugation at 5,000 × *g* for 10 min at 4 °C, the proteins were hydrolyzed *in vacuo* with 2 ml of 6 N HCl for 24 h at 110 °C. The hydrolysates were then dried and dissolved in sodium citrate buffer, pH 3.15. The amino acid analysis was performed using a JEOL JLC-500

amino acid analyzer equipped with a JEOL LC30-DK20 data analyzing system.

Preparation of Monoclonal Antibody against 2-Nonenal-modified Protein—The immunogen was prepared by incubating the KLH (1.0 mg/ml) with 10 mM 2-nonenal in 3 ml of PBS at 37 °C for 24 h. We immunized the female BALB/c mice (Chubu Kagaku Shizai Co., Ltd., Nagoya, Japan) on day 1 with complete Freund adjuvant and 0.06 mg of immunogen (2-nonenal-modified KLH) and boosted on days 11, 21, and 31 with incomplete Freund adjuvant and 0.02 mg of immunogen by emulsifying and intraperitoneal injection. Titers to 2-nonenal-modified BSA in the immunized mice sera were measured by an enzyme-linked immunosorbent assay (ELISA) (15). Two months after the initial immunization, the immunized mice were given an intraperitoneal boost of 0.06 mg/ml 2-nonenal-modified KLH. Three days later, the spleen cells from the immunized mice were fused with P3/U1 murine myeloma cells in the presence of polyethylene glycol and cultured in hypoxanthine/amethopterin/thymidine selection medium. The culture supernatants of the hybridoma were screened using an ELISA, employing pairs of wells of microtiter plates on which were absorbed 2-nonenal-treated BSA as the antigen (0.5 μg of protein/well). After incubation with 100 μl of the hybridoma supernatants, and with intervening washes with PBS/Tween, the wells were incubated with alkaline phosphatase-conjugated goat anti-mouse IgG, followed by a substrate solution containing 0.5 mg/ml 1,2-phenylenediamine. Hybridoma cells corresponding to the supernatants that were positive on the 2-nonenal-modified BSA and negative on the native BSA were then cloned by limited dilution. After repeated screening, four clones were obtained. Among them, clone 27Q4 showed the most significant recognition of the 2-nonenal-modified BSA. Competitors were prepared by incubating 50 mM amino acid derivatives, N^{α}-acetyl-L-lysine, N^{α}-acetylhistidine, or N^{α}-acetylcysteine, in the presence or absence of 2-nonenal (50 mM), in 50 mM sodium phosphate buffer, pH 7.2, for 24 h at 37 °C.

Isolation and Structural Analysis of Antigenic 2-Nonenal-Lysine Adducts—The reaction mixture (6 ml) contained 200 mM *trans*-2-nonenal and 200 mM N^{α}-acetyl-L-lysine in 50 mM sodium phosphate buffer, pH 7.2. After incubation for 72 h at 37 °C, a portion of the reaction mixture was analyzed by a reverse-phase HPLC using a Develosil ODS-HG-5 column (4.6 × 250 mm, Nomura Chemicals) equilibrated in a solution of 5% acetonitrile in 0.01% trifluoroacetic acid. The chromatographic separation was performed by a gradient elution as follows (solvent A was water and solvent B was acetonitrile, both containing 0.01% trifluoroacetic acid): 0–10 min, linear gradient to 40% B; 10–40 min, 40% B; 40–41 min, linear gradient to 100% B; 41–45 min, hold; flow rate = 0.8 ml/min. The isolation and purification of the antigenic adducts (**P-1** and **P-2**) were carried out under the same HPLC conditions and finally obtained 2.3 and 2.9 mg of **P-1** and **P-2**, respectively. Their structures were characterized by LC/MS and ^{1}H and ^{13}C NMR. The LC/MS was measured by a Jasco PlatformII-LC instrument. The LC/MS analysis was performed using a Develosil ODS-HG-5 column (4.6 × 250 mm) eluted with a linear gradient from 100% water containing 0.1% acetic acid to 100% acetonitrile containing 0.1% acetic acid for 60 min at a flow rate of 0.8 ml/min. The elution profiles were monitored by absorbance at 239 nm. The NMR analyses were performed using a Bruker AMX400 (400 MHz) instrument. For **P-1**, ^{1}H NMR (400 MHz, MeOD): δ 0.85–0.92 (6H, m), 1.25–1.50 (22H, m), 1.66 (2H, m), 1.70–2.08 (7H, m), 2.13 (2H, q), 2.87 (2H, t), 4.36 (1H, q), 4.55 (2H, t), 6.16 (1H, m), 6.51 (1H, d, J = 11.6 Hz), 7.93 (1H, d, J = 6.4 Hz), 8.66 (1H, s), and 8.70 (1H, d, J = 5.4 Hz). For **P-2**, ^{1}H NMR (MeOD, 600 MHz): δ 0.89–0.94 (6H, m), 1.30–1.52 (11H, m), 1.40–1.52 (2H, m), 1.56 (2H, m), 1.66 (2H, m), 1.70–1.92 (2H, m), 1.96 (3H, s), 2.01–2.06 (2H, m), 2.36 (2H, q), 2.93 (2H, t), 4.39 (1H, q), 4.53 (2H, q), 6.54 (1H, m), 6.66 (1H, d, J = 16.2 Hz), 7.84 (1H, d, J = 6.0 Hz), 8.61 (1H, d, J = 6.0 Hz), 8.91 (1H, s); ^{13}C NMR (150 MHz, MeOD): δ 14.3 (2C), 22.4, 23.4, 23.5 (2C), 29.5, 30.0, 30.2, 31.6, 32.1, 32.5, 32.6, 34.0, 34.2, 53.0, 62.0, 122.4, 129.2, 139.4, 142.2 (2C), 142.5, 160.7, 173.3, and 175.1.

Immunohistochemical Detection of 2-Nonenal Adducts in Vivo—Male Wistar rats (Shizuoka Laboratory Animal Center, Shizuoka, Japan), weighing 130–150 g (6 weeks old), were used. The animals received a single intraperitoneal injection of Fe^{3+}-NTA (15 mg of iron/kg of body weight) or repeated administration as described previously (5). They were sacrificed by decapitation at 0, 1, 6, 24, and 48 h after a single injection or 3 weeks after the repeated administration. Both kidneys of each animal were immediately removed. One of them was fixed in Bouin's solution, embedded in paraffin, cut in 3-mm thick slices, and used for the immunohistochemical analyses by an avidin-biotin complex method with alkaline phosphatase. Briefly, after deparaffinization with xylene and ethanol, normal rabbit serum (Dako; diluted to 1:75) for the inhibition of the nonspecific binding of the secondary antibody, a primary antibody (20 μg/ml), biotin-labeled rabbit anti-mouse IgG serum (Vector Laboratories; diluted to 1:300), and avidin-biotin complex (Vector; diluted to 1:100) were sequentially used. Procedures, using PBS or the IgG fraction (0.5 mg/ml) of the normal mouse serum instead of mAb 27Q4, showed no response or negligible positive responses.

Preparation of Isotope-labeled HPH-lysines—To prepare the [U-$^{13}C_6$,$^{15}N_2$]HHP-lysine, 1 mM N^{α}-[U-$^{13}C_6$,$^{15}N_2$]Fmoc-N^{ε}-Boc-lysine was treated with 1 ml of trifluoroacetic acid for 2 h at room temperature, applied to a C-18 Sep-Pak column, and eluted with 5 ml of methanol. The eluate was evaporated and redissolved in 1 ml of 50 mM sodium phosphate buffer, pH 7.4. The obtained N^{α}-[U-$^{13}C_6$,$^{15}N_2$]Fmoc-lysine was modified with 1 mM 2-nonenal for 24 h at 37 °C and subsequently treated with 20% piperidine for 2 h at room temperature to remove the Fmoc moiety. The resulting mixture was purified by HPLC, carried out under the same HPLC conditions as already described. LC/ESI/MS/MS analysis with MRM mode of the isotope-labeled HPH-lysines showed that that the standards contained no endogenous (nonlabeled) adducts (supplemental Fig. S1).

LC/ESI//MS/MS—Mass spectrometric analyzes were performed using a Quattro Ultima triple stage quadrupole mass spectrometer (Waters-Micromass, Manchester, UK) equipped with an ESI probe and interfaced with a Shimadzu HPLC system (Shimadzu, Kyoto, Japan). The sample injection volumes of 20 μl each were separated on a Shim-pack VP-ODS 2.0 × 150 mm, 5-μm column (Shimadzu) at a flow rate of 0.3 ml/min. A

discontinuous gradient was used by solvent A (H_2O containing 0.1% formic acid) with solvent B (acetonitrile) as follows: isocratic elution with 20% solvent B from 0 to 5 min; increasing to 50% solvent B from 5 to 20 min; increasing to 70% solvent B from 20 to 25 min; and then isocratic elution with 70% solvent B from 25 to 30 min. Mass spectrometric analyzes were performed on line using ESI/MS/MS in the positive ion mode with MRM mode (cone potential 35 eV/collision energy 24 eV). The MRM transitions monitored were as follows: [U-$^{13}C_6$,$^{15}N_2$]HHP-lysine, *m/z* 397 → 261; *cis*- and *trans*-HHP-lysine, *m/z* 389 → 260. L-Glutamate upon reaction with 2-nonenal gave similar MRM transitions but MRM transitions (360 → 260) were detected in the reaction mixture of 2-nonenal/glutamate; however, their elution times were completely different from those of standard HHP-lysines (supplemental Fig. S2). The amount of each HHP-lysine adduct was quantified by the ratio of the peak area of the target adducts and of the HHP-lysine-stable isotope. The HHP-lysine standard concentration was determined by assay of the amino groups using a 2,4,6-trinitrobenzenesulfonic acid assay (16). Briefly, to 30 μl of hydrolyzed HHP-lysine solution was added 30 μl of 4% $NaHCO_3$ and 30 μl of 0.1% 2,4,6-trinitrobenzenesulfonic acid. The solution was allowed to react at 37 °C for 2 h, and 30 μl of 1% SDS and 15 μl of 1 N HCl were then added. The absorbance of the solution was read at 340 nm. The standard curve (using valine as a standard) was linear in the range 0–3.3 nmol of NH_2. QuanLynx (version 4.0) software (Waters-Micromass) was used to create standard curves (supplemental Fig. S3) and to calculate the adduct concentrations.

For the LC/ESI/MS/MS analysis of the HHP-lysines *in vitro*, the protein samples were treated with an equal volume of 20% trichloroacetic acid. After centrifugation at 5,000 × *g* for 10 min at 4 °C, the proteins were hydrolyzed *in vacuo* with 2 ml of 6 N HCl for 24 h at 110 °C. The internal standard, [U-$^{13}C_6$,$^{15}N_2$]HHP-lysine, was added to the samples prior to the acid hydrolysis. After the acid hydrolysis, the samples were partially separated with Oasis hydrophilic-lipophilic balance (HLB) cartridges (Waters, Milford, MA). After the sample loading, the HLB cartridges were washed with 2 ml of 50% methanol, and the HHP-lysines were eluted with 2 ml of 80% methanol. The samples were then dried, dissolved in methanol, and subjected to LC/ESI/MS/MS analysis.

For the LC/ESI/MS/MS analyses of the HHP-lysines *in vivo*, male ddY mice (Shizuoka Laboratory Animal Center, Shizuoka), weighing 25–35 g (6 weeks of age), were used. Animals received a single intraperitoneal injection of Fe^{3+}-NTA (5 mg of iron/kg of body weight). They were sacrificed at 0, 1, 3, 6, and 24 h after the administration. Both kidneys of each animal were immediately removed. The kidneys were homogenized in a Teflon homogenizer in 10 volumes of PBS containing butylated hydroxytoluene (1 mM). The homogenate was centrifuged at 18,000 × *g* for 15 min, and the precipitates were hydrolyzed *in vacuo* with 6 N HCl (2 ml) and [U-$^{13}C_6$,$^{15}N_2$]HHP-lysine for 24 h at 110 °C. The hydrolysates were then dried and dissolved in methanol. After the acid hydrolysis, the samples were partially separated with HLB cartridges and subjected to LC/ESI/MS/MS analysis.

DiD-labeled AcLDL Uptake Assays—DiD (1,1′-dioctadecyl-3,3,3′,3′-tetramethylindodicarbocyanine perchlorate)-labeled AcLDL was prepared from human LDL according to the methods previously described for 1,1′-dioctadecyl-3, 3,3′,3′-tetramethylindocarbocyanine perchlorate labeling (17). CHO cells that stably expressed CFP-tagged LOX-1 (18) were grown on coverslips. For the cells transiently expressing CFP, CHO cells suspended at a density of 1 × 10^4 cells/ml were plated on a coverslip 24 h prior to transfection. The cells (40% confluent) were transfected with pECFP-N1 (Clontech) using Lipofectamine reagent according to the manufacturer's protocol and then incubated for 48 h. Cells were treated with each concentration of adducts prepared in F-12 medium without fetal calf serum for 10 min at 37 °C in a 5% CO_2 humidified atmosphere, followed by incubation with DiD-AcLDL (0.4 μg/coverslip) for another 15 min. The cells were then fixed with 2% formaldehyde. Each coverslip was inverted onto a glass slide with a spacer, and the cells were examined using a Leica DM IRE2 microscope (Leica Microsystems, Wetzler, Germany) equipped with a ×100, NA 1.4 objective and a Cool SNAP-HG digitalized cooled CCD camera (Roper Scientific, Trenton, NJ) driven by MetaMorph software (Universal Imaging, Downingtown, PA). The expression level of LOX-1 was examined by the CFP fluorescence intensity using an E4 filter with excitation at 436 nm (7-nm bandpass) and a 470-nm long pass emission filter. Images were acquired at 0.2 s exposure time. The DiD-AcLDL uptake was analyzed by the amount of the DiD-derived fluorescence intensity using a Y5 filter, with excitation using a 620 nm (50-nm bandpass) and 700 nm (75-nm bandpass) emission filters. The images were acquired at a 2-s exposure.

Images of over 100 cells from three independent experiments were acquired. After subtracting the background emission level with respect to 436 and 620 nm from the fluorescence image, the fluorescence intensity of each cell was determined from the average pixel value of the whole cell. The expression level of LOX-1 was calculated from the CFP intensity, and the level of uptake of AcLDL was calculated from the DiD intensity (18). For each experimental condition, the level of AcLDL uptake was averaged per expression level of LOX-1.

RESULTS

Monoclonal Antibody against Protein-bound 2-Nonenal—To assess the reactivity of 2-nonenal to proteins, HSA (1 mg/ml) was exposed to 2-nonenal (0–10 mM) under physiological conditions *in vitro*, and changes in the amino acid composition of the protein were examined by an amino acid analysis. As shown in Fig. 1*B*, 2-nonenal preferentially reacted with the lysine residues, indicating that 2-nonenal can covalently modify protein spontaneously, and the likely mechanism is a nucleophilic attack by the protein.

To determine whether modification of proteins by 2-nonenal occurs *in vivo*, we attempted to develop a mAb against 2-nonenal-modified protein. To this end, the keyhole limpet hemocyanin that had been exposed to 2-nonenal was administered to mice at 10-day intervals. During the preparation of the mAb, hybridomas were selected by comparing the reactivities of the culture supernatant to the 2-nonenal-modified BSA. Among the four obtained clones, the clone 27Q4 showed the most dis-

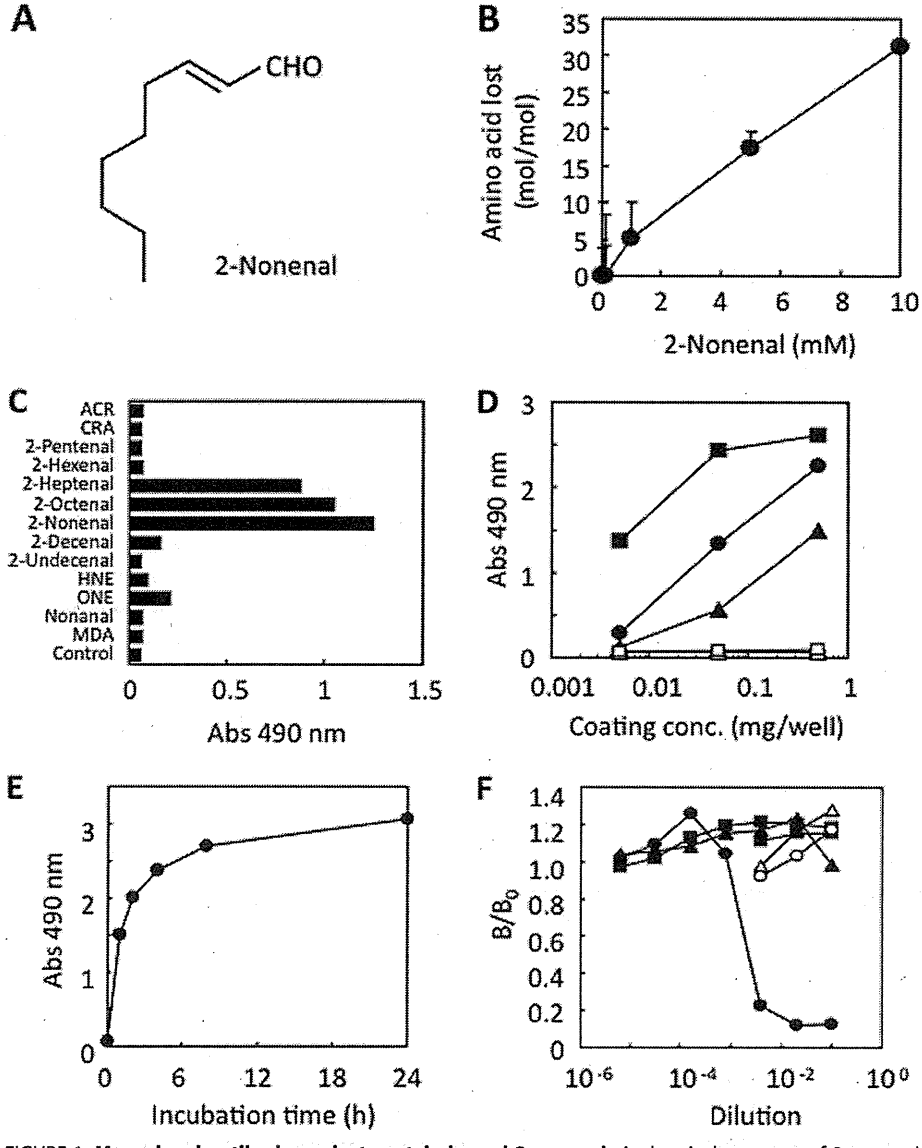

FIGURE 1. **Monoclonal antibody against protein-bound 2-nonenal.** *A*, chemical structure of 2-nonenal. *B*, loss of lysine residues in protein treated with 2-nonenal. HSA (1 mg/ml) was incubated with 0–10 mM 2-nonenal in 50 mM sodium phosphate buffer, pH 7.2, at 37 °C. *C*, immunoreactivity of mAb 27Q4 to aldehyde-modified proteins. Affinity of mAb 27Q4 was determined by a direct ELISA using aldehyde-modified BSA as the absorbed antigen. A coating antigen (0.5 μg/well) was prepared by incubating 1 mg of BSA with 1 mM aldehydes in 1 ml of 50 mM sodium phosphate buffer, pH 7.2, for 24 h at 37 °C. *ACR*, acrolein; *CRA*, crotonaldehyde; *MDA*, malondialdehyde; *HNE*, 4-hydroxy-2-nonenal; *ONE*, 4-oxo-2-nonenal. *D*, immunoreactivity of mAb 27Q4 to 2-nonenal-modified proteins. A coating antigen (0.005–0.5 μg/well) was prepared by incubating 1 mg of protein with 1 mM 2-nonenal in 1 ml of 50 mM sodium phosphate buffer, pH 7.2, for 24 h at 37 °C. Proteins are as follows: *open square*, native lactoglobulin; *closed triangle*, 2-nonenal-modified HSA; *closed circle*, 2-nonenal-modified BSA; *closed square*, 2-nonenal-modified lactoglobulin. *E*, time-dependent increase in the immunoreactivity of protein treated with 2-nonenal. HSA (1 mg/ml) was incubated with 1 mM 2-nonenal in 50 mM sodium phosphate buffer, pH 7.2, at 37 °C. *F*, competitive ELISA analysis with the reaction mixtures of amino acid derivatives and 2-nonenal. Competitors were prepared by incubating 50 mM amino acid derivatives, N^{α}-acetyllysine, N^{α}-acetylhistidine, or N^{α}-acetylcysteine, in the presence or absence of 2-nonenal (50 mM), in 50 mM sodium phosphate buffer, pH 7.2, for 24 h at 37 °C. Competitors are as follows: *open circle*, N^{α}-acetyllysine; *open triangle*, N^{α}-acetylhistidine; *open square*, N^{α}-acetylcysteine; *closed circle*, 2-nonenal/N^{α}-acetyllysine; *closed triangle*, 2-nonenal/N^{α}-acetylhistidine; *closed square*, 2-nonenal/N^{α}-acetyllysine.

tinctive recognition of the 2-nonenal-modified BSA. The specificity of the obtained antibody was characterized. As shown in Fig. 1*C*, the monoclonal antibody showed a strong immunoreactivity not only with 2-nonenal but also with 2-octenal and 2-heptenal, whereas the unmodified BSA was not recognized by the antibody. We then determined whether the 2-nonenal-modified proteins contained the 27Q4 epitope. The mAb 27Q4 immunoreacted with not only 2-nonenal/BSA, but also with 2-nonenal/HSA and 2-nonenal/lactoglobulin, whereas the unmodified proteins were not recognized by the antibody (Fig. 1*D*), suggesting that the 2-nonenal-modified proteins contained a common adduct structure recognized by mAb 27Q4. The time course study of formation of the 2-nonenal epitope during the incubation of BSA with 2-nonenal *in vitro* was determined by direct ELISA using mAb 27Q4. When BSA was incubated with 1 mM 2-nonenal at 37 °C, the immunoreactive materials rapidly increased within 4 h (Fig. 1*E*). To identify the possible attacking nucleophiles that form antigenic structures, we investigated the reaction of 2-nonenal with individual amino acids likely to form stable antigenic products. We studied lysine, histidine, and cysteine, each protected at the α-amino group as an acetamide, leaving only the side-chain nucleophile as a potential reactant. As shown in Fig. 1*F*, binding of the 2-nonenal-modified protein to the antibody was hardly inhibited by the reaction mixtures of 2-nonenal/histidine and 2-nonenal/cysteine but was significantly inhibited by the reaction mixture of 2-nonenal/lysine, suggesting that the mAb might recognize a 2-nonenal-lysine adduct as the epitope. None of the original amino acid derivatives, histidine, cysteine, and lysine, cross-reacted with mAb 27Q4.

Isolation and Structural Characterization of the Antigenic 2-Nonenal-Lysine Adducts—Because characterization of the ability of antibodies to recognize specific molecular targets in their native three-dimensional conformation is critical to the use of these reagents, we sought to identify the intrinsic epitope recognized by mAb 27Q4. To identify the 2-nonenal-lysine adduct recognized by mAb 27Q4, the immunoreactivity with the reaction products of 2-nonenal with N^{α}-acetyllysine was characterized. As shown in Fig. 2*A*, the ELISA analysis of the HPLC fractions for immuno-

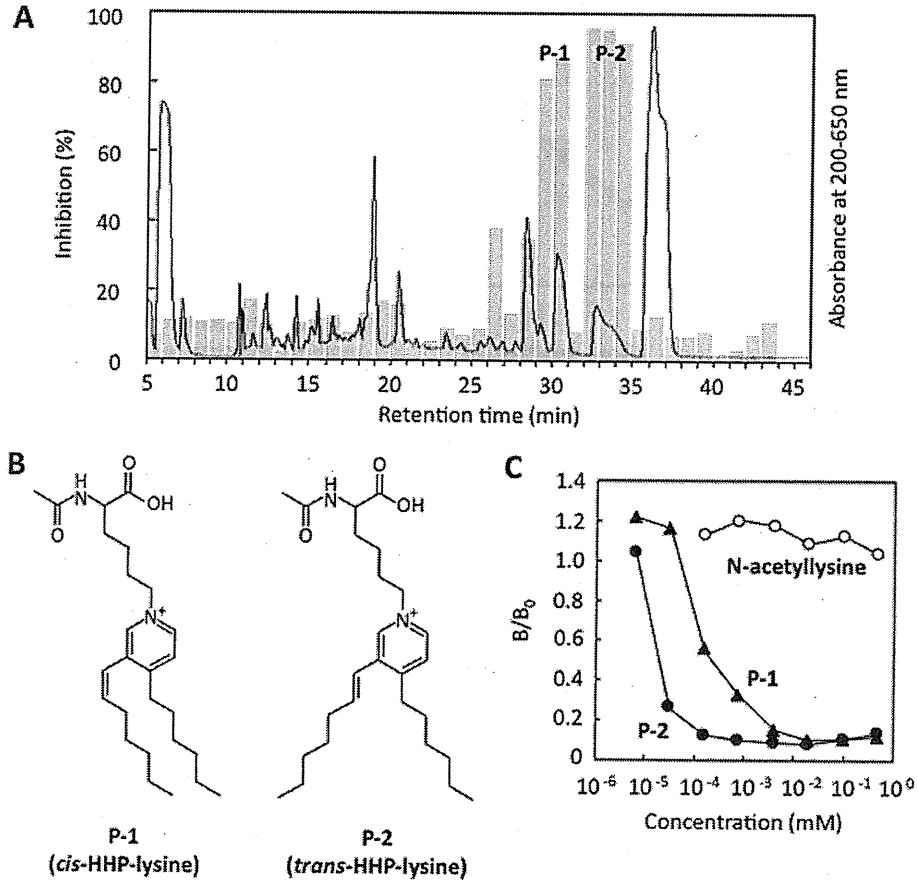

FIGURE 2. **Isolation and structural characterization of the antigenic 2-nonenal-lysine adducts.** *A*, competitive ELISA analysis of HPLC fractions for immunoreactivity with mAb 27Q4. The reaction was performed by incubating 200 mM N^{α}-acetyllysine with 200 mM 2-nonenal in 1 ml of 50 mM sodium phosphate buffer, pH 7.2, at 37 °C for 24 h. *Solid line*, profile of UV absorbance at 200–650 nm. *Bar*, competitive ELISA analysis. *B*, chemical structures of *cis*-HHP-lysine and (**P-1**) and *trans*-HHP-lysine (**P-2**). *C*, competitive ELISA analysis with *cis*- and *trans*-HHP-lysine. Competitors are as follows: *closed circle*, N^{α}-acetyl-*trans*-HHP-lysine (**P-2**); *closed triangle*, N^{α}-acetyl-*cis*-HHP-lysine (**P-1**); *open circle*, N^{α}-acetyllysine.

reactivity with mAb 27Q4 showed that the antibody primarily had an immunoreactivity with two fractions, **P-1** and **P-2**. The LC/MS total ion current analysis of **P-2** detected one product, which showed a 242-Da increase in the mass value of the unmodified lysine derivative and gave the $[M + H]^+$ peak at *m/z* 431.0 (supplemental Fig. S4), suggesting that it was composed of one molecule of N^{α}-acetyllysine and two molecules of 2-nonenal.

Because **P-2** was a major immunoreactive fraction, we first attempted to identify this product. To characterize the chemical structure, isolation by HPLC on the reverse-phase column was carried out. After purification, the structure of the products was characterized by an NMR analysis. The assignments of protons and carbons were based on the result of the HMBC and distortionless enhancement by polarization transfer experiments. Compared with the ^{13}C NMR and ^{1}H NMR spectra between N^{α}-acetyllysine and the product (supplemental Figs. S5–S10), the Cb (173.3 ppm), the Cd (175.1 ppm), the Ha proton (1.96 ppm), and the Hc proton (δH 4.39 ppm; δC 53.0 ppm) remained in the ^{13}C NMR and ^{1}H NMR spectra of the product. The correlation spectroscopy spectrum showed correlations between the Hc proton with the He (δH 1.70–1.92 ppm; δC 32.1 ppm) proton, the He proton with the Hf proton (δH 1.40–1.52 ppm; δC 23.4 or 23.5 ppm), the Hf proton with the Hg proton (δH 2.01–2.06 ppm; δC 31.6 ppm), and the Hg proton with the Hh proton (δH 4.53 ppm; δC 62.0 ppm). The ^{13}C NMR spectrum of the product showed five signals (δC 129.2, 139.4, 142.2 (two carbon signals), and 160.7 ppm) in the aromatic carbon region. In the HMBC spectrum, cross-peaks between the δ-proton of the lysine residue, Hh, and carbons (Hh-Ci (142.2 ppm) and Hh-Cm (142.2 ppm)), cross-peaks between Hi (8.61 ppm, $J = 6.0$ Hz) and carbons (Hi-Ch, Hi-Cj (129.2 ppm) and Hi-Ck (160.7 ppm)), and cross-peaks between Hm (8.91 ppm) with carbons (Hm-Ch, Hm-Ci, Hm-Ck, and Hm-Cl (139.4 ppm)). The coupling constant and HMBC spectrum indicated that Hi and Hj (7.84 ppm, $J = 6.0$ Hz) are adjacent. Moreover, in the HMBC spectrum, the cross-peaks Hj and carbons (Hj-Ci, Hj-Ck, and Hj-Cl) are observed. The Ck and Cl were missing from the distortionless enhancement by polarization transfer spectrum. This indicates that Ck and Cl are quaternary carbons. These results suggest that the aromatic part of this product seemed to be a pyridinium ring, in which Ck and Cl are substituted. The coupling constant for the vinyl proton (Ht, 6.66 ppm) was $J = 16.2$ Hz for the *trans*-proton. In the HMBC spectrum, the cross-peaks between the Ht and carbons (Ht-Ck, Ht-Cl, and Ht-Cm) and cross-peaks between the Hn and carbons (Hn-Cj, Hn-Ck, and Hn-Cl) were observed. These results indicated that the substituted quaternary carbons, Ck and Cl, were adjacent to Cn and Ct, respectively. The residual parts of **P-2** were the (*E*)-1-heptenyl and hexyl groups. The signals at 0.89–0.94 ppm were assigned to Hs and Hz. The correlation spectroscopy experiments were performed to determine the alkyl chain connectivity. With the correlation spectroscopy spectrum, starting from the methyl groups, the spin systems for an (*E*)-1-heptenyl chain and a hexyl chain were determined. After establishing the connectivities for the alkyl chains, the HMBC experiments were performed. Based on these characteristics, it was determined that **P-2** was the novel 2-nonenal-lysine adduct, N^{α}-acetyl-N^{ε}-3-[(hept-1-enyl)-4-hexylpyridinium]lysine (N^{α}-acetyl-HHP-lysine) (Fig. 2*B*). The LC/MS total ion current analysis of **P-1** detected one product, which showed a 242-Da increase in the mass value of the unmodified lysine derivative and gave the $[M + H]^+$ peak at *m/z* 430.9 (supplemental Fig. S11), suggesting that **P-1** is a *cis* isomer of N^{α}-acetyl-HHP-lysine. To confirm the structure of **P-1**, the

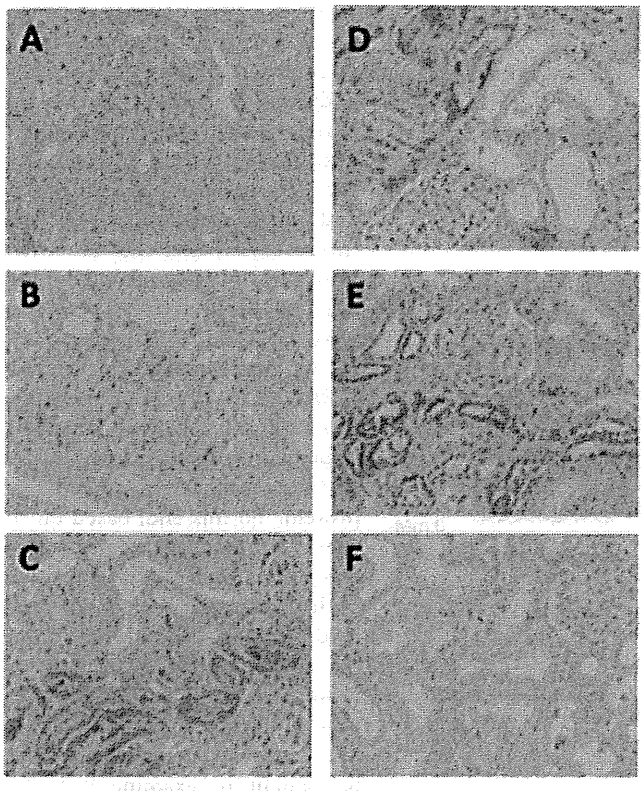

FIGURE 3. **Immunohistochemistry of renal cortex with mAb 27Q4 (×400).** *A*, untreated control; *B*, 1 h; *C*, 6 h; *D*, 24 h; *E*, 48 h after single intraperitoneal injection of Fe^{3+}-NTA; *F*, 3 weeks after repeated intraperitoneal injection of Fe^{3+}-NTA. Refer to "Experimental Procedures" for details.

NMR experiments were performed (supplemental Figs. S12–S17) and showed that the coupling constant for the vinyl proton (6.51 ppm) was $J = 11.6$ Hz for the *cis* proton. Selected ion-current chromatograms obtained from the LC/MS analysis showed that, when 200 mM N^{α}-acetyllysine was incubated with 200 mM 2-nonenal for 72 h, **P-1** and **P-2** were formed in the ratio of 1:1.4, indicating that the *cis* isomer of N^{α}-acetyl-HHP-lysine can be formed from the *trans*-2-nonenal-mediated reaction.

As shown in Fig. 2*C*, the antibody showed a specificity toward both **P-1** and **P-2** but was rather specific to **P-2**. Approximately 50 pmol of **P-2**/well (100 μl) caused a 50% inhibition of the antibody binding to the 2-nonenal-modified protein, whereas at least 100-fold higher concentrations of **P-1** were necessary for the same inhibition.

Formation of Immunoreactive Materials with mAb 27Q4 in Vivo—We next sought to explore whether immunoreactive materials with mAb 27Q4 are formed *in vivo*. For this purpose, we used Fe^{3+}-NTA-treated rats, an established animal model of oxidant injury to the kidney. It has been established that Fe^{3+}-NTA induces acute renal proximal tubular necrosis, a consequence of oxidative tissue damage, that eventually leads to a high incidence of renal adenocarcinoma in rodents (11). Previously, we have shown that the levels of 2-nonenal markedly increase after the administration of Fe^{3+}-NTA (5). In the control rat kidney (Fig. 3*A*), an almost negligible level of immunoreactivity was observed. The immunoreactivities were found in some of the renal proximal tubular cells 1, 6, 24, and 48 h (Fig. 3, *B–E*) after the administration of 15 mg of iron/kg of body weight of Fe^{3+}-NTA. No immunoreactivity was observed after the repeated (3 weeks) administrations of Fe^{3+}-NTA (Fig. 3*F*). These patterns of distribution in the rat kidney are consistent with those of the distribution of membrane lipid peroxidation products and their conjugates with cytosolic proteins, suggesting a correlation between the production of the 2-nonenal/2-alkenals and oxidative stress. Pre-absorption of the antibody with HHP-lysine completely abolished the immunostaining (data not shown).

LC/ESI/MS/MS Analysis of HHP-lysine—To obtain direct evidence for the formation of the antigenic HHP-lysine adducts *in vivo*, we first attempted to establish a method for the detection of adducts using LC/ESI/MS/MS. The acid hydrolysis of N^{α}-acetyl-HHP-lysine gave a single product, which was identified to be the expected de-acetylated product (HHP-lysine) (supplemental Figs. S18 and S19). Collision-induced dissociation of the HHP-lysine produced relevant daughter ions at *m/z* 344, 260, 130, and 84 (Fig. 4*A*). These ions were applied to the structure shown in Fig. 4*B*. The product ions at *m/z* 84 and 130 were confirmed to be the product ions of a lysine moiety, and the ions at *m/z* 344 and 389 originated from the HHP-lysine. Fig. 4*C* demonstrates the LC/ESI/MS/MS analysis of the HHP-lysine (0–10 nM) in the positive ion mode using MRM between the transition from the protonated parent ion $[M + H]^+$ to the characteristic daughter ion (*m/z* 389.6 → 260.2), allowing detection of both the *cis*- and *trans*-HHP-lysines. Chromatograms for the internal standard are shown in supplemental Fig. S20. Using the LC/ESI/MS/MS technique, we attempted to detect HHP-lysine in the 2-nonenal-modified HSA. No adducts were detected in the native HSA, whereas the treatment of HSA with 0–10 mM 2-nonenal in 50 mM sodium phosphate buffer, pH 7.2, for 24 h at 37 °C gave 0.61 and 0.86 mol of the *cis*- and *trans*-HHP-lysines, respectively, per mol of protein (Fig. 4, *D* and *E*).

In Vivo Formation of HHP-lysine via Lipid Peroxidation—It is known that 2-nonenal is generated by the lipid peroxidation of unsaturated fatty acids, such as palmitoleic acid (6). To examine the involvement of the lipid peroxidation during the formation of HHP-lysine, we sought to detect HHP-lysine in the Cu^{2+}-oxidized LDL using LC/ESI/MS/MS. Incubation of LDL with Cu^{2+} led to the oxidation of the LDL as assessed by the formation of thiobarbituric acid-reactive substances (data not shown). As shown in Fig. 5*A*, the Cu^{2+}-induced peroxidation of LDL dramatically enhanced the formation of HHP-lysine with the levels of the *trans*-HHP-lysine exceeding those of the *cis*-HHP-lysine by 2-fold.

To further examine which fatty acids are involved in the formation of the HHP-lysine, several unsaturated fatty acids were incubated with an iron/ascorbate-mediated free radical generating system in the presence of HSA, and HHP-lysine generated on the protein molecule was analyzed by LC/ESI/MS/MS following acid hydrolysis. As shown in Fig. 5*B*, the iron/ascorbate-mediated oxidation of palmitoleic acid and ω6-polyunsaturated fatty acids, such as linoleic acid, γ-linolenic acid, and arachidonic acid, in the presence of HSA resulted in a dramatic

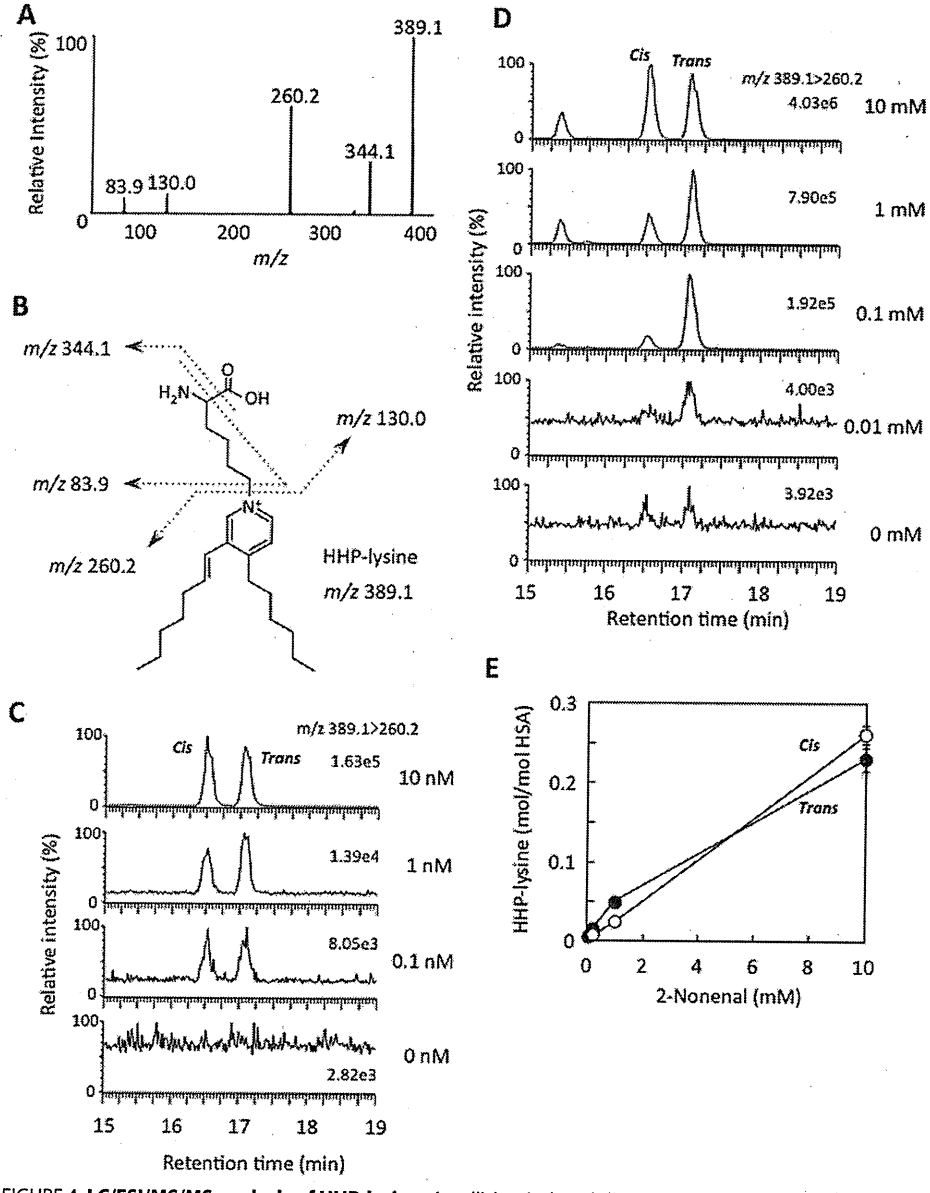

FIGURE 4. **LC/ESI/MS/MS analysis of HHP-lysine.** *A*, collision-induced dissociation of the $[M + H]^+$ of *trans*-HHP-lysine at *m/z* 389.5 at a collision energy of 25 V. *B*, proposed structures of individual ions. *C*, LC/ESI/MS/MS analysis of authentic *cis*- and *trans*-HHP-lysines. The ion current tracing of HHP-lysine using LC/ESI/MS/MS with MRM is shown. *D*, LC/ESI/MS/MS analysis of *cis*- and *trans*-HHP-lysines generated in the 2-nonenal-modified HSA. The ion current tracing of *cis*- and *trans*-HHP-lysines using LC/ESI/MS/MS with MRM is shown. *E*, dose-dependent formation of *cis*- and *trans*-HHP-lysines in the 2-nonenal-modified HSA. Symbols used are as follows: *open circle*, *cis*-HHP-lysine; *closed circle*, *trans*-HHP-lysine. *D* and *E*, HSA (1.0 mg/ml) was incubated with 2-nonenal (0–10 mM) in 50 mM sodium phosphate buffer, pH 7.2, for 24 h at 37 °C. The native and modified HSA were analyzed by LC/ESI/MS/MS with MRM mode followed by acid hydrolysis.

increase in the levels of HHP-lysine with levels of *trans*-HHP-lysine exceeding those of *cis*-HHP-lysine by 3–9-fold.

We then sought to explore whether HHP-lysine is formed in the kidney of animals exposed to Fe^{3+}-NTA *in vivo*. Kidneys from the untreated and treated animals collected 1 and 3 h after the administration of Fe^{3+}-NTA were analyzed for HHP-lysine using LC/ESI/MS/MS. The MRM transitions monitored were as follows: [U-$^{13}C_6$,$^{15}N_2$]HHP-lysine, *m/z* 397 → 261; *cis*- and *trans*-HHP-lysine, *m/z* 389 → 260. Multiple distinct MRM channels (parent 389.1 → 344.1, 260.2, 130.0, and 83.9) showed that each of the appropriate transitions showed co-chromatography (supplemental Figs. S21 and S22). In addition, the ratio of the different parent → daughter transitions was also checked (Fig. 5*C*). As shown in Fig. 5*D*, the levels of both the *cis*- and *trans*-HHP-lysines markedly increased 3 h after the administration of Fe^{3+}-NTA. The yields of the *cis*- and *trans*-HHP-lysines at 3 h were 366.5 and 357.8 fmol/g wet tissue weight, respectively.

Recognition of the 2-Nonenal-Lysine Adduct by LOX-1—Finally, we evaluated the biological implication of the 2-nonenal modification of protein. To this end, based on the previous findings that a scavenger receptor LOX-1 might be involved in the processing of aldehyde-modified proteins (19) and that, among the aldehyde-treated proteins, the 2-nonenal-modified protein can be very efficiently incorporated into the LOX-1-overexpressing cells,[3] we sought to examine if LOX-1 recognizes the 2-nonenal-lysine adduct. AcLDL was used as an alternative ligand to the oxidized LDL, which shows a comparable affinity to LOX-1 (20) to avoid ambiguous effects from variations in the extent of the oxidized LDL oxidation (21, 22). In this assay, the amount of incorporated DiD-labeled AcLDL directly reflected the binding activity of LOX-1, which was confirmed by an independent analysis as described previously (23). The rate of DiD-AcLDL taken up by CHO stably expressing CFP/LOX-1 was assessed by a fluorescence microscope equipped with a cooled CCD camera. In CHO cells transfected with pECFP-N1, the CFP signal was detected in the cytoplasm, and no DiD-AcLDL uptake was detected (Fig. 6*A*, *top*). The stable cell line expressed a moderate amount of LOX-1, and a fluorescence derived from DiD-AcLDL was observed (Fig. 6*A*, *middle*). The effect of the 2-nonenal-modified BSA upon DiD-AcLDL uptake through LOX-1 was examined in the competition assay to evaluate the LOX-1 recognition of modified proteins. The native BSA failed to show any inhibitory effects (date not shown), whereas the protein modi-

[3] S. Machida and K. Uchida, manuscript in preparation.

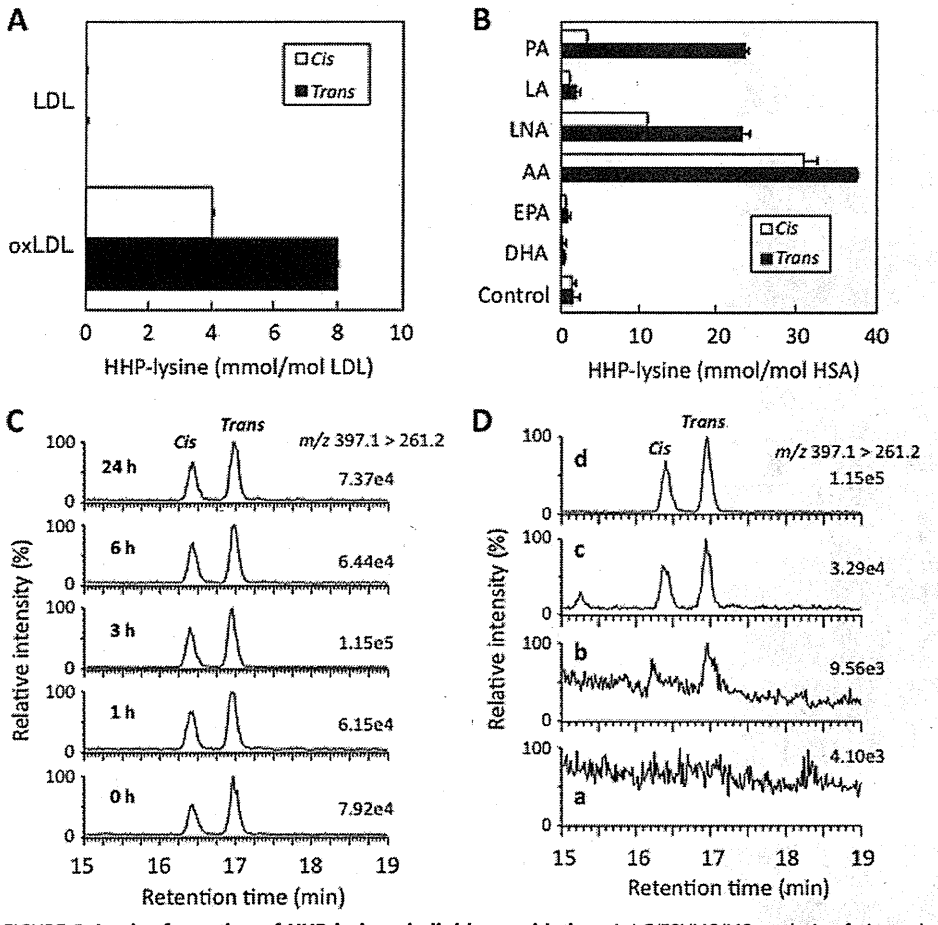

FIGURE 5. ***In vivo* formation of HHP-lysine via lipid peroxidation.** *A*, LC/ESI/MS/MS analysis of *cis*- and *trans*-HHP-lysines in oxidized LDL (*oxLDL*). LDL (0.5 mg) was incubated with 5 μM Cu^{2+} in 1 ml of PBS at 37 °C. The native LDL and oxidized LDL were analyzed by LC/ESI/MS/MS with MRM mode followed by acid hydrolysis. *B*, LC/ESI/MS/MS analysis of *cis*- and *trans*-HHP-lysines in protein exposed to lipid peroxidation. The metal-catalyzed oxidation of unsaturated fatty acids in the presence of HSA was performed by incubating HSA (1 mg/ml) with 2 mM unsaturated fatty acids in the presence of 50 μM Fe^{2+} and 1 mM ascorbic acid in 1 ml of 50 mM sodium phosphate buffer, pH 7.2, in atmospheric oxygen at 37 °C. The native and modified HSA were analyzed by LC/ESI/MS/MS with MRM mode followed by acid hydrolysis. The abbreviations used are as follows: *PA*, palmitoleic acid; *LA*, linoleic acid; *LNA*, γ-linolenic acid; *AA*, arachidonic acid; *EPA*, eicosapentaenoic acid; *DHA*, docosahexaenoic acid. *C*, LC/ESI/MS/MS analysis of *cis*-[U-$^{13}C_6$,$^{15}N_2$]- and *trans*-[U-$^{13}C_6$,$^{15}N_2$]HHP-lysines in the kidneys of mice exposed to Fe^{3+}-NTA. The ion current tracing of *cis*-[U-$^{13}C_6$,$^{15}N_2$]- and *trans*-[U-$^{13}C_6$,$^{15}N_2$]HHP-lysines LC/ESI/MS/MS with MRM is shown. *D*, LC/ESI/MS/MS analysis of *cis*- and *trans*-HHP-lysines in the kidneys of mice exposed to Fe^{3+}-NTA. The ion current tracing of HHP-lysine using LC/ESI/MS/MS with MRM is shown. *Panel a*, 0 h after administration; *panel b*, 1 h after administration; *panel c*, 3 h after administration; *panel d*, internal standards.

fied with 2-nonenal significantly inhibited the uptake of AcLDL (Fig. 6*A*, *bottom*). Finally, we evaluated the purified *cis*- and *trans*-HHP-lysines for their recognition by LOX-1 in the competition assay, and we observed that they served as a ligand for LOX-1, as evidenced by their ability to effectively compete with AcLDL (Fig. 6, *B–D*). There was no effect by the 1% DMSO carried from the stock solution of the HHP-lysine (data not shown).

DISCUSSION

Lipid peroxidation proceeds by a free radical chain reaction mechanism and yields lipid hydroperoxides as major initial reaction products. Subsequently, the decomposition of the lipid hydroperoxides generates a number of breakdown products that display a wide variety of damaging actions. A number of reactive aldehydes derived from lipid peroxidation have been implicated as causative agents in cytotoxic processes initiated by the exposure of biological systems to oxidizing agents (2). On the basis of a large number of reports concerning the detection of lipid peroxidation-specific adducts as biomarkers in human diseases, there is no doubt that the steady-state levels of lipid peroxidation products increase in pathophysiological states associated with oxidative stress. Considerable progress has also recently been made toward understanding the mechanisms of action of lipid peroxidation products. The quantitative and analytical importance of lipid peroxidation-specific adducts has prompted the development of methods to specifically analyze these adducts to understand their chemical nature, formation pathway, and distribution level *in vivo*.

The results presented herein show that 2-nonenal, a body odorant originating from lipid peroxidation, covalently modifies proteins. A spontaneous chemical reaction was observed *in vitro*. In addition, we obtained a murine monoclonal antibody, mAb 27Q4, that clearly distinguished the 2-nonenal-modified protein from the native protein. This antibody appeared to be highly specific for the protein-bound 2-alkenals, including 2-heptenal, 2-octenal, and 2-nonenal. Using the antibody, the formation of the 2-nonenal-modified proteins *in vivo* was tested in the kidney of rats exposed to Fe^{3+}-NTA. The iron chelate was originally used for an experimental model of iron overload (24). Repeated intraperitoneal injections of Fe^{3+}-NTA were reported to induce acute and subacute renal proximal tubular necrosis and a subsequent high incidence (60–92%) of renal adenocarcinoma in male rats and mice (25, 26). A single injection of Fe^{3+}-NTA causes a number of time-dependent morphological alterations in the structure and the function of the renal proximal tubular cells and their mitochondria. During the early stage of injury, typical cellular changes are the loss of the brush border, cytoplasmic vesicles, mitochondrial disorganization, and dense cytoplasmic deposits in the proximal tubular cells. Most of the damaged epithelia show the typical appearance of necrotic cells, and more than half of the proximal tubular cells are gone. It has been suggested that oxidative stress is one of the basic mechanisms of Fe^{3+}-NTA-in-

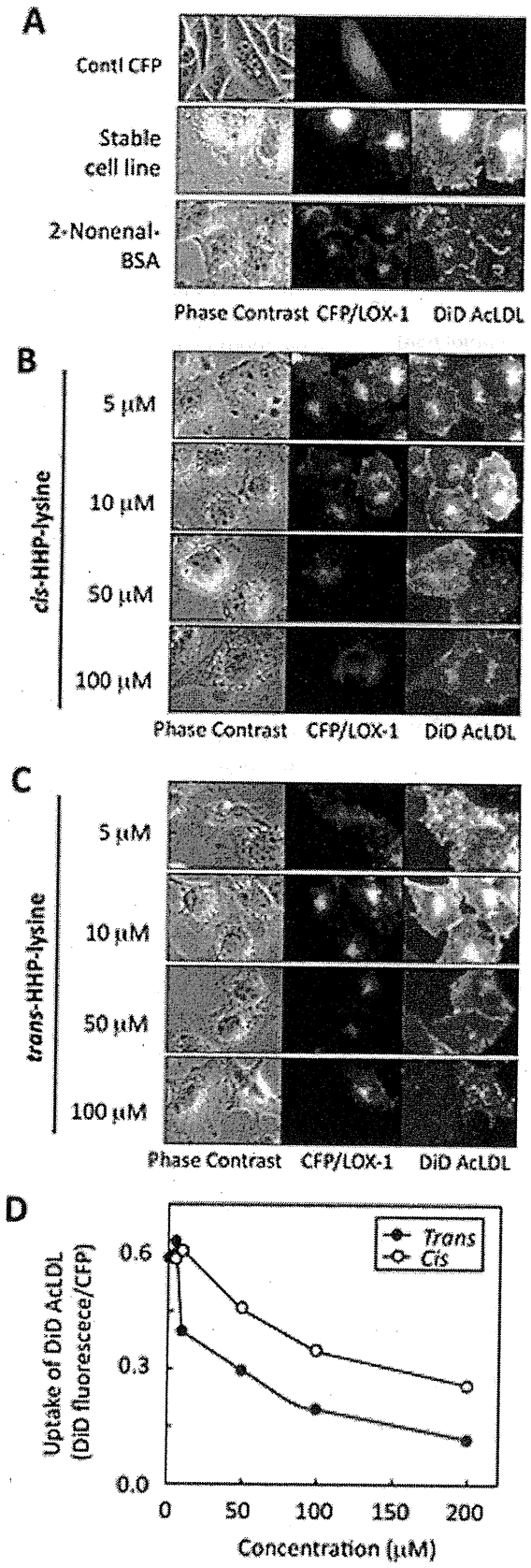

duced acute renal injury and is closely associated with renal carcinogenesis (27, 28). The present *in vivo* study has shown that lipid peroxidation generates 2-nonenal covalently bound to proteins in the renal proximal tubules of rats treated with Fe^{3+}-NTA (Fig. 3). To the best of our knowledge, this is the first report of the *in vivo* formation of protein-bound 2-nonenal/2-alkenals in the target organ of the carcinogenic protocol. It was also striking that the immunoreactivities with mAb 27Q4 were detected even 48 h after the administration of Fe^{3+}-NTA (Fig. 3*E*). Long retention of this aldehyde may play a role in the Fe^{3+}-NTA-induced renal carcinogenesis.

Upon investigation of an antigenic adduct recognized by the antibody (mAb 27Q4), we unexpectedly identified novel lysine-pyridinium adducts, *cis*- and *trans*-HHP-lysines. Of interest, the monoclonal antibodies raised against protein-bound 2-alkenals, such as acrolein and crotonaldehyde, recognize pyridinium-containing adducts as the major epitopes (29, 30). It is likely that, due to the placement of a fixed, positive charge on the ϵ-amino group, the pyridinium-containing adducts could be an important immunological epitope generated in 2-alkenal-modified proteins. The formation of the 3,4-substituted pyridinium adducts has also been reported to be a dominant pathway for modification of the primary amine with 2-alkenals, such as 2-hexenal and 2-octenal (31, 32). Based on these studies, HHP-lysine is likely to be formed through the formation of the 2-nonenal-lysine Schiff base (Fig. 7). After the formation of the Schiff base adduct, the C3 position of the initial Schiff base may be attacked by the C2 of the enolate anion from the second aldehyde, followed by dehydration and cyclization to form the isomeric pyridinium adduct. On the other hand, *trans-cis* isomerization of α,β-unsaturated compounds is known to be catalyzed by amines (addition-elimination). Thus, the isomerization required for the formation of *cis*-HHP-lysine may occur at the stage of the free 2-nonenal or following Schiff base formation.

Due to the fact that the core structures of the pyridinium-containing lysine adducts are resistant to the conventional acid hydrolysis of proteins, we established a highly sensitive method for the detection of *cis*- and *trans*-HHP-lysine using LC/ESI/MS/MS. *In vitro* studies of the detection of HHP-lysine demonstrated that the 2-nonenal-lysine adducts were generated in the oxidized LDL (Fig. 5*A*). In addition, substantial amounts of the 2-nonenal-lysine adducts, mainly the *trans*-HHP-lysine, were detected in the metal-catalyzed peroxidation of unsaturated

FIGURE 6. **Effect of the 2-nonenal-lysine adducts on ligand uptake by LOX-1.** *A*, CHO cells transfected with vector carrying only CFP (*top*). LOX-1 expression level and AcLDL uptake ability of stable cell line (*middle*) is shown. Effect of 2-nonenal-modified BSA (4 μg/ml) on AcLDL uptake (*bottom*) is shown. *B*, effect of *cis*-HHP-lysine (10–100 μM) on AcLDL uptake. *C*, effect of *trans*-HHP-lysine (10–100 μM) on AcLDL uptake. Images were acquired using ×100 objective. *Panels* are as follows: *left*, phase contrast; *middle*, CFP/LOX-1 (excitation at 436 nm; exposure time, 0.2 s); *right*, DiD-AcLDL (excitation at 620 nm; exposure time, 2 s). *D*, quantitative measurement of fluorescence intensity of each cell. CHO cells stably expressing CFP/LOX-1 were treated with each concentration of adducts and followed by incubation with DiD-AcLDL. The cell-associated fluorescence intensity derived from CFP and DiD (pixel value) was determined as described under "Experimental Procedures." The specific uptake was expressed as the fluorescence intensity derived from DiD (pixel value) per the fluorescence intensity derived from CFP (pixel value) of each cell. The values represent the means of over 100 cells from three independent experiments.

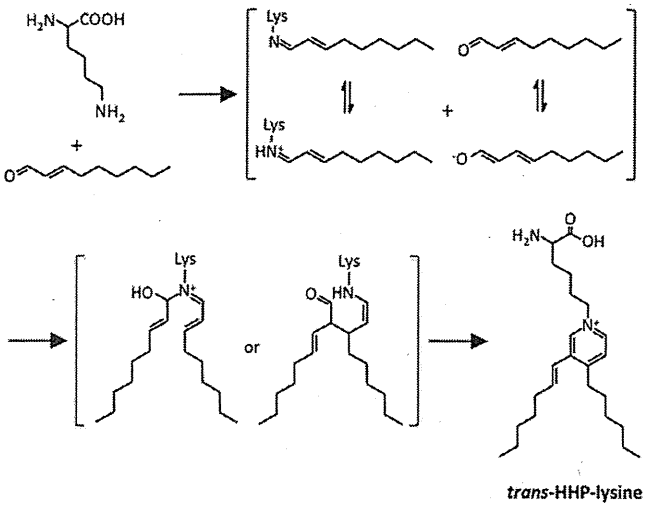

FIGURE 7. **Proposed mechanism for the formation of HHP-lysine.**

fatty acids in the presence of protein (Fig. 5*B*). These data suggest that covalent modification of proteins by 2-nonenal, generating the pyridinium-containing lysine adducts, could have diagnostic applications. Because oxidative degradation of unsaturated fatty acids, accelerated by lipid peroxides, may be involved in the formation of 2-nonenal, resulting in deterioration of the body odors for the middle-aged and the elderly (6), plasma or red blood cell levels of a long-lived 2-nonenal adduct could provide a measure of past exposure and aid in the management of one's health condition. Such a reporter function would be analogous to the use of glycated hemoglobin as a marker of past hyperglycemia and a guide to the management of diabetes.

It should also be noted that peroxidation of not only palmitoleic acid, but also ω6-polyunsaturated fatty acids, such as linoleic acid, γ-linolenic acid, and arachidonic acid, in the presence of HSA generated HHP-lysine. 2-Nonenal was previously identified as an unpleasant greasy and grassy odor component endogenously generated during the peroxidation of palmitoleic acid (6). However, until this study, *bona fide* unsaturated fatty acids responsible for the formation of 2-nonenal have remained unidentified. Therefore, this study has established that ω6-polyunsaturated fatty acids also represent an excellent source of 2-nonenal. Although the mechanism of the formation of 2-nonenal during lipid peroxidation has not yet been experimentally resolved, there may be no doubt that 2-nonenal could be ubiquitously generated under oxidative stress.

Scavenger receptors have been shown to bind aldehyde-modified proteins (33–37). These receptors are thought to provide a mechanism for the clearance of these modified proteins from the circulation through a number of cell types. Indeed, a previous study has shown that endothelial cells can bind and degrade an aldehyde-modified protein (38). In this study, to determine whether the 2-nonenal-specific epitopes enter cells though scavenger receptors, we selected LOX-1 and performed inhibition studies. We showed that BSA incubated with 2-nonenal significantly inhibited the LOX-1-mediated uptake of AcLDL (Figs. 6 and 7). In addition, we directly assessed whether HHP-lysine might serve as a ligand and observed that both the *cis*- and *trans*-HHP-lysines competed for the uptake of AcLDL. These data suggested that LOX-1 might serve as a receptor for the 2-nonenal-lysine adducts generated on oxidized LDL molecules. Data from the mesenteric vein injection of an aldehyde-modified protein also suggest that LOX-1 may be involved to a certain degree in these processes (38). Thus, it is likely that LOX-1 is involved in the recognition of 2-nonenal-modified proteins. However, the possibility still exists for other receptors to be involved in the processing of 2-nonenal-modified proteins.

In summary, to assess the formation of 2-nonenal generation under oxidative stress *in vivo*, we raised a new murine monoclonal antibody, mAb 27Q4, against the 2-nonenal-modified KLH. The model system provides a detailed structural characterization of the epitopes, the *cis*- and *trans*-HHP-lysines, formed during the reaction of the lysine side-chain amino groups with 2-nonenal. We proved that the immunoreactive materials with mAb 27Q4 were indeed generated in an animal model of oxidative stress *in vivo*. In addition, using LC/ESI/MS/MS, the biological levels of the 2-nonenal-lysine adduct *in vitro* and *in vivo* were accurately estimated. Finally, we examined the involvement of the scavenger receptor LOX-1 in the recognition of 2-nonenal-modified proteins and established that the receptor recognized the HHP-lysine adducts as a ligand. The present results not only offer structural insights into protein modification by lipid peroxidation products but also provide a platform for the chemical analysis of protein-bound aldehydes *in vitro* and *in vivo*.

REFERENCES

1. Halliwell, B., and Gutteridge, J. M. (1989) *Free Radicals in Biology and Medicine*, 2nd Ed., Clarendon Press, Oxford
2. Esterbauer, H., Schaur, R. J., and Zollner, H. (1991) *Free Radic. Biol. Med.* **11,** 81–128
3. Uchida, K. (2000) *Free Radic. Biol. Med.* **28,** 1685–1696
4. Marnett, L. J., Riggins, J. N., and West, J. D. (2003) *J. Clin. Invest.* **111,** 583–593
5. Toyokuni, S., Luo, X. P., Tanaka, T., Uchida, K., Hiai, H., and Lehotay, D. C. (1997) *Free Radic. Biol. Med.* **22,** 1019–1027
6. Haze, S., Gozu, Y., Nakamura, S., Kohno, Y., Sawano, K., Ohta, H., and Yamazaki, K. (2001) *J. Invest. Dermatol.* **116,** 520–524
7. Hernández-Hernández, A., Sánchez-Yagüe, J., Martín-Valmaseda, E. M., and Llanillo, M. (1999) *Free Radic. Biol. Med.* **26,** 1218–1230
8. Ohyashiki, T., Kamata, K., Takeuchi, M., and Matsui, K. (1995) *J. Biochem.* **118,** 508–514
9. Sawamura, T., Kume, N., Aoyama, T., Moriwaki, H., Hoshikawa, H., Aiba, Y., Tanaka, T., Miwa, S., Katsura, Y., Kita, T., and Masaki, T. (1997) *Nature* **386,** 73–77
10. Chen, X. P., Zhang, T. T., and Du, G. H. (2007) *Cardiovasc. Drug Rev.* **25,** 146–161
11. Toyokuni, S., Uchida, K., Okamoto, K., Hattori-Nakakuki, Y., Hiai, H., and Stadtman, E. R. (1994) *Proc. Natl. Acad. Sci. U.S.A.* **91,** 2616–2620
12. De Montarby, L., Mosset, P., and Gree, R. (1988) *Tetrahedron Lett.* **29,** 3937–3940
13. Rindgen, D., Nakajima, M., Wehrli, S., Xu, K., and Blair, I. A. (1999) *Chem. Res. Toxicol.* **12,** 1195–1204
14. Marnett, L. J., and Tuttle, M. A. (1980) *Cancer Res.* **40,** 276–282
15. Toyoda, K., Nagae, R., Akagawa, M., Ishino, K., Shibata, T., Ito, S., Shibata, N., Yamamoto, T., Kobayashi, M., Takasaki, Y., Matsuda, T., and Uchida, K. (2007) *J. Biol. Chem.* **282,** 25769–25778
16. Habeeb, A. F. (1966) *Anal. Biochem.* **14,** 328–336
17. Stephan, Z. F., and Yurachek, E. C. (1993) *J. Lipid Res.* **34,** 325–330
18. Matsunaga, S., Xie, Q., Kumano, M., Niimi, S., Sekizawa, K., Sakakibara, Y.,

Komba, S., and Machida, S. (2007) *Exp. Cell Res.* **313,** 1203–1214
19. Duryee, M. J., Klassen, L. W., Freeman, T. L., Willis, M. S., Tuma, D. J., and Thiele, G. M. (2003) *Biochem. Pharmacol.* **66,** 1045–1054
20. Shi, X., Niimi, S., Ohtani, T., and Machida, S. (2001) *J. Cell Sci.* **114,** 1273–1282
21. Lougheed, M., and Steinbrecher, U. P. (1996) *J. Biol. Chem.* **271,** 11798–11805
22. Yoshida, H., Kondratenko, N., Green, S., Steinberg, D., and Quehenberger, O. (1998) *Biochem. J.* **334,** 9–13
23. Chen, M., Nagase, M., Fujita, T., Narumiya, S., Masaki, T., and Sawamura, T. (2001) *Biochem. Biophys. Res. Commun.* **287,** 962–968
24. Awai, M., Narasaki, M., Yamanoi, Y., and Seno, S. (1979) *Am. J. Pathol.* **95,** 663–673
25. Ebina, Y., Okada, S., Hamazaki, S., Ogino, F., Li, J. L., and Midorikawa, O. (1986) *J. Natl. Cancer Inst.* **76,** 107–113
26. Li, J. L., Okada, S., Hamazaki, S., Ebina, Y., and Midorikawa, O. (1987) *Cancer Res.* **47,** 1867–1869
27. Toyokuni, S. (1996) *Free Radic. Biol. Med.* **20,** 553–566
28. Toyokuni, S. (2009) *Cancer Sci.* **100,** 9–16
29. Furuhata, A., Ishii, T., Kumazawa, S., Yamada, T., Nakayama, T., and Uchida, K. (2003) *J. Biol. Chem.* **278,** 48658–48665
30. Ichihashi, K., Osawa, T., Toyokuni, S., and Uchida, K. (2001) *J. Biol. Chem.* **276,** 23903–23913
31. Baker, A., Zídek, L., Wiesler, D., Chmelík, J., Pagel, M., and Novotny, M. V. (1998) *Chem. Res. Toxicol.* **11,** 730–740
32. Alaiz, M., and Barragan, S. (1995) *Chem. Phys. Lipids* **77,** 217–223
33. Brown, M. S., Basu, S. K., Falck, J. R., Ho, Y. K., and Goldstein, J. L. (1980) *J. Supramol. Struct.* **13,** 67–81
34. Horiuchi, S., Murakami, M., Takata, K., and Morino, Y. (1986) *J. Biol. Chem.* **261,** 4962–4966
35. Takata, K., Horiuchi, S., Araki, N., Shiga, M., Saitoh, M., and Morino, Y. (1988) *J. Biol. Chem.* **263,** 14819–14825
36. Takata, K., Horiuchi, S., Araki, N., Shiga, M., Saitoh, M., and Morino, Y. (1989) *Biochim. Biophys. Acta* **986,** 18–26
37. Steinbrecher, U. P., Lougheed, M., Kwan, W. C., and Dirks, M. (1989) *J. Biol. Chem.* **264,** 15216–15223
38. Duryee, M. J., Freeman, T. L., Willis, M. S., Hunter, C. D., Hamilton, B. C., 3rd, Suzuki, H., Tuma, D. J., Klassen, L. W., and Thiele, G. M. (2005) *Mol. Pharmacol.* **68,** 1423–1430

SAR and QSAR in Environmental Research
Vol. 22, Nos. 5–6, July–September 2011, 505–523

Taylor & Francis
Taylor & Francis Group

Application of chemical reaction mechanistic domains to an ecotoxicity QSAR model, the KAshinhou Tool for Ecotoxicity (KATE)

A. Furuhama[a]*, K. Hasunuma[a], Y. Aoki[a], Y. Yoshioka[b] and H. Shiraishi[a]

[a]*Research Center for Environmental Risk, National Institute for Environmental Studies (NIES), Tsukuba, Japan;* [b]*Faculty of Education and Welfare Science, Oita University, Oita, Japan*

(*Received 12 October 2010; in final form 1 February 2011*)

The validity of chemical reaction mechanistic domains defined by skin sensitisation in the Quantitative Structure–Activity Relationship (QSAR) ecotoxicity system, KAshinhou Tools for Ecotoxicity (KATE), March 2009 version, has been assessed and an external validation of the current KATE system carried out. In the case of the fish end-point, the group of chemicals with substructures reactive to skin sensitisation always exhibited higher root mean square errors (RMSEs) than chemicals without reactive substructures under identical C- or log *P*-judgements in KATE. However, in the case of the *Daphnia* end-point this was not so, and the group of chemicals with reactive substructures did not always have higher RMSEs: the Schiff base mechanism did not function as a high error detector. In addition to the RMSE findings, the presence of outliers suggested that the KATE classification rules needs to be reconsidered, particularly for the amine group. Examination of the dependency of the organism on the toxic action of chemicals in fish and *Daphnia* revealed that some of the reactive substructures could be applied to the improvement of the KATE system. It was concluded that the reaction mechanistic domains of toxic action for skin sensitisation could provide useful complementary information in predicting acute aquatic ecotoxicity, especially at the fish end-point.

Keywords: KATE; chemical reaction mechanistic domain; ecotoxicity; applicability domain

1. Introduction

Risk management of new and existing chemical substances is a significant issue in the construction of an environmentally sustainable society. To resolve unsustainable patterns of consumption and production, in 2002 the World Summit on Sustainable Development [1] adopted a plan, 'aiming to achieve, by 2020, that chemicals are used and produced in ways that lead to the minimization of significant adverse effects on human health and the environment'. In June 2007 a new chemical substances regulation – Registration, Evaluation, Authorization and Restriction of Chemicals (REACH) – was implemented by the European Union [2]. Moreover, in Japan the Chemical Substances Control Laws (CSCLs) have very recently been amended to produce a comprehensive system for the control of chemicals [3]. Under the requirements for risk management, the [Quantitative] Structure–Activity Relationship ([Q]SAR) plays an important role in filling the gaps in knowledge for chemicals so far untested in the laboratory, and may yield the information

*Corresponding author. Email: ayako.furuhama@nies.go.jp

ISSN 1062-936X print/ISSN 1029-046X online

DOI: 10.1080/1062936X.2011.569944
http://www.informaworld.com

for prioritising the chemicals to be tested [4]. For instance, the usefulness of QSAR in aquatic toxicity has been reviewed, particularly in the context of the REACH legislation [5].

The principles of (Q)SAR have also been discussed by the Organisation for Economic Co–operation and Development (OECD) [6], and one of its five validation principles is that a (Q)SAR should have a defined domain of applicability. A definition of "applicability domain" has been provided by Netzeva et al. [7]: 'The applicability domain of a (Q)SAR is the response and chemical structure space in which the model makes predictions with a given reliability'. Consequently the applicability domain may in practice guarantee the performance of toxic predictions. For example, various response domain spaces with more than one descriptor have recently been introduced and utilised [7–11]. Furthermore, on the basis of the descriptor, chemical structural space and so on, QSAR software that includes aquatic toxicity prediction capability, such as TIssue MEtabolism Simulator (TIMES) [12,13], provides an indication of whether a predicted chemical is in-domain or out-of-domain based on the descriptor and chemical structural space. The KAshinhou Tool for Ecotoxicity (KATE) system [14,15], which provides ecotoxicity QSAR models for 96-h fish LC_{50} and 48-h *Daphnia* EC_{50} end–points, also has domains for evaluating the predicted results. Model users can confirm the reliability of a prediction by the domain information, in addition to the QSAR statistical data.

We have investigated the efficiency of the additional domains for fish and *Daphnia* end-points in the current KATE (March 2009 version) system. In particular, chemical reaction mechanistic domains defined by skin sensitisation [16] were targeted in order to enhance reliability. Skin sensitisation, and aquatic reactive toxicity, i.e. fish, are different end-points, but the protein-binding reaction mechanisms show similar behaviour; consequently dependence on electrophilic reactivity is found for both end-points [17,18]. Moreover, research into the prediction of skin sensitisation potency has been very active over the past few years [16,19–24]. Aptula et al. have examined the relationship between the electrophilic reactivity of a chemical and its skin sensitisation potential [16,19]. Recently, Enoch et al. [25] have used SMiles ARbitrary Target Specification (SMARTS®) [26] patterns to describe structural fragments (substructures) on the basis of information provided by Aptula et al. [16]. In the system of Enoch et al. [25], their set of patterns was assessed for its ability to correctly identify potential mechanisms within the 208 training dataset; by using a knowledge of organic chemistry, the applicability domain within each mechanism was expanded as far as possible.

Note that the SMARTS patterns allow the specification of substructures by using rules that are straightforward extensions of the Simplified Molecular Input Line Entry Specification (SMILES®) notation [27] for chemical substances. Because KATE uses the same SMILES linear notation to predict aquatic toxicity, the SMARTS patterns can easily be applied to detect the reactive substructures of chemicals without the need for stereochemical information.

2. Methodology

2.1 *Definition of reaction mechanistic domains*

We have used the reactive patterns in Table 2 of the paper by Enoch at al. [25] to define chemical reaction mechanistic domains (described in the present article simply as "reactive domains"). We were fortunate in being able to obtain the raw data used by Enoch et al. in

their study [25] and translate the original SMARTS patterns into the classification algorithm, Fragment Identification by Tree Structure (FITS), developed by Yoshioka [28–30]. FITS is able to detect the substructure in the SMILES strings and is the main engine of the current KATE system for the classification rule and the definition of structure domains (i.e. *C*-judgement, Section 2.2 in the present article [14]).

We shall concentrate here on the "reactive" compounds with the patterns of the following reactions [16]: Michael-type addition (MA), pro-MA, aromatic nucleophilic substitution (S_NAr), aliphatic nucleophilic substitution (S_N2), Schiff base formation (SB), pro-SB and acylation. Unfortunately, the pro-S_N2 SMART patterns of the Enoch paper [25], expressing anthracene and phenanthrene substructures, are not definable, for technical reasons associated with the current FITS. Notably, the pro-MA, pro-SB and pro-S_N2 patterns indicate the substructures convertible to those of the corresponding parent electrophilic compounds by metabolism [31,32]. Moreover, substructures designated "reactive" signify only the reactive domain of the defined SMARTS patterns. The designation "non-reactive" denotes compounds without the pattern defined by the above domains.

2.2 *KATE and its domains*

This section provides a review of the KATE system. KATE was developed using the database on aquatic toxicity results gathered on fish (*Oryzias latipes*) and *Daphnia* (*Daphnia magna*) by the Japanese Ministry of the Environment (MoE) [33], and the United States Environmental Protection Agency (US EPA) fathead minnow (*Pimephales promelas*) database [34,35]. In order to construct QSAR models for toxicity prediction, the chemicals in the reference dataset were classified by their substructures, which meant that the classification rules could define the structural spaces of each QSAR model. The equations of the models were linearly correlated with the octanol–water partition coefficient (log *P*) values, with the exception of the equation for the *neutral organics* class, which was an aggregate of the chemicals in the defined classes. These classification rules and equations have appeared in a previous article [14]. In addition, internal validation had earlier shown that acceptable results were given by QSAR models of KATE with more than a 0.5 root mean square error (RMSE), a squared correlation coefficient (r^2) of up to 0.7, and more than five reference data ($n > 5$) [14]. Since acute aquatic QSAR had been developed over more than 30 years, some of the classification rules for the QSAR models in KATE followed similar concepts to those of other aquatic QSAR models based on chemical substructures [5,35–44].

Log *P*- and *C*-judgements are also key features of the KATE system. The former judgement is based on the descriptor log *P* range defined by the reference data of the class (shown in Tables 1 and 2 of Furuhama et al. [14]) to which the chemical belongs. The latter is categorised as a structural domain and is defined by the substructures (specified functional groups) shown in Appendix 3 of Furuhama et al. [14]. The definition of the *C*-judgement is as follows: *C(1)* is the in-domain of the *C*-judgement, defined as all substructures of a test chemical found in reference chemicals in the class. *C(2)* is the in-domain of the *C*-judgement, defined as all substructures of a test chemical found in reference chemicals either in its class or in the class, *neutral organics*. External validation indicated that the group of chemicals in the in-domain of the *C*-judgement had lower RMSE than the group without considering the *C*-judgement [14].

Table 1. Numbers of chemical compounds evaluated.

		KATE domain					
End-point		*all*	*C(2)*	*C(1)*	*log P*	*log P C(2)*	*log P C(1)*
Fish	*Chemicals*	57	39	32	44	33	26
	Predicted	64	44	36	49	38	30
Daphnia	*Chemicals*	78	49	35	52	35	26
	Predicted	86	54	40	58	40	31

Note: *Chemicals*: Number of chemicals in the training set with toxicities to be predicted by KATE in the present study.
Predicted: Total number of predicted toxicity values. Because some chemicals belonged to more than one class, the *Predicted* category was larger than *Chemicals*. When a chemical was found to belong to more than one QSAR class, all the predicted data were adopted. If only the name of the class was available, such data were omitted.
All: Both in-domain and out-of-domain data for log *P*- and log *C*-judgements are included.
log P: In-domain of log *P*-judgement.
C(2): In-domain of *C*-judgement is defined as all the substructures of a test chemical in reference chemicals in either the *neutral organics* class or the class of the test.
C(1): In-domain of *C*-judgement is defined as all the substructures of a test chemical found in reference chemicals in the class.
The domain notation is also defined in the text and in Table 3 of a previous study [14].

2.3 *Test dataset for the present study*

As test sets for our study (Table 1), we selected the Japan MoE dataset of chemicals available after March 2009. The test sets therefore did not include any of the reference data in the March 2009 version of KATE. The ecotoxicity test sets (96-h LC_{50} fish and 48-h EC_{50} *Daphnia*) discussed here have already been published on the Japanese MoE website [33]. The input log *P* values for the toxicity calculation were obtained from the US EPA KOWWIN® [45]. SMILES notations of the predicted chemicals were defined by the system in the Estimation Program Interface (EPI) Suite® [46] and the stand-alone version, KATE on PAS. The predicted toxicity value, log *P*-judgement and *C*-judgement were obtained from the internet version, KATE on NET (March 2009 version) [15].

3. Results and discussion

The predicted toxicities, the log *P* and *C*-judgements and the reactive domains from the skin sensitisation information are summarised in Tables 2 (fish) and 3 (*Daphnia*). When test chemicals are allocated to two or more classes, all the classes have been evaluated during the study. Similarly, when a chemical is categorised as having more than one reactive domain, all reactive mechanisms were listed. For example, 3-formyl-6-*iso*-propylchromone (Figure 1) has two reactive substructures, and is listed as "SB, Michael" in the right column of Table 2.

In the current test dataset, chemicals with in-domain of log *P* and *C(1)* judgements tended to be classified as "non-reactive". If these judgements are ignored, in the predicted fish toxicity values 27 and 37 chemicals were categorised as "reactive" or "non-reactive", respectively, and the equivalent numbers for *Daphnia* were 29 and 57. When only the

Table 2. Results of KATE-based predictions, with CAS number, chemical name, toxicity of chemicals to fish as measured and as predicted by KATE, log *P*- and *C*-judgements (KATE domains), and "reactive" mechanistic domains (Enoch et al. [25]) for the 57 compounds in the test set.[1]

CAS	Chemical name	log P Pred.	KATE class name	log (1/LC_{50} [mM]) Pred.	log (1/LC_{50} [mM]) Meas.	Domain log P^2	Domain C^3	'reactive'[4]
286–62–4	Cyclooctene oxide	2.64	Epoxides (Clog P)	1.91	−0.20	O	*C (1)*	S_N2
2425–79–8	1,4-Bis (2,3-epoxypropoxy)butane	−0.15	Epoxides (Clog P)	1.01	1.19	X	*C (1)*	S_N2
111–30–8	Glutaraldehyde	−0.18	Aldehydes	0.19	1.06	O	*C (1)*	SB
1540–36–9	2,4-Pentanedione, 3-butyl-	1.94	Conjugated systems2	1.75	−0.13	O	*C (1)*	SB
487–68–3	2,4,6-Trimethylbenzaldehyde	3.35	Aldehydes	1.90	1.09	X	*C (1)*	SB
4067–16–7	Pentaethylenehexamine	−3.67	Hydrazines (Clog P)	0.30	0.04	X	X	pro-S_N2
6117–91–5	2-Buten-1-ol	0.63	Conjugated systems2	1.18	1.26	O	*C (1)*	pro-Michael
20103–09–7	2,5-Dichloro-1,4-benzenediamine	0.90	Amines aromatic or phenols1	2.67	0.91	O	*C (1)*	pro-Michael
101–96–2	1,4-Benzenediamine, *N,N'*-bis (1-methylpropyl)-	3.50	Amines aromatic or phenols1	2.65	2.77	O	X	pro-Michael
51963–82–7	Benzenamine, 2,5-diethoxy-4-(4-morpholinyl)-	2.01	Amines aromatic or phenols1	2.66	1.08	O	X	pro-Michael
40220–08–4	Tris(2-hydroxyethyl)isocyanuric acid acrylate	3.75	Amides and imides	1.77	1.79	O	X	Michael, acylating
40220–08–4	Tris(2-hydroxyethyl)isocyanuric acid acrylate	3.75	Acrylates	2.09	1.79	X	X	Michael, acylating
100–43–6	4-Vinylpyridine	1.71	Hydrocarbons aromatic	0.19	2.02	O	*C (1)*	Michael
1855–63–6	1-Cyclohexene-1-carbonitrile	2.04	Neutral organics	0.04	0.42	O	*C (1)*	Michael
1335–46–2	Methylionone	4.84	Conjugated systems2	3.01	1.84	X	*C (1)*	Michael
1855–63–6	1-Cyclohexene-1-carbonitrile	2.04	Nitriles aliphatic	0.56	0.42	O	*C (2)*	Michael
406–86–0	4,4,4-Trifluorocrotonitrile	1.04	Halides2	0.54	2.78	O	*C (2)*	Michael
98–81–7	α-Bromostyrene	3.29	Unclassified	1.55	3.09	O	X	Michael
117–80–6	2,3-Dichloro-1,4-naphthoquinone	2.65	Halides1	2.00	3.86	O	X	Michael
483–63–6	*N*-Ethyl-*N*-crotonoyl-2-toluidine	2.73	Amides and imides	1.01	0.43	O	X	Michael
569–64–2	CI Basic Green 4	0.80	Amines aromatic or phenols5	−0.18	3.42	O	X	Michael
16669–59–3	*N*- (Isobutoxymethyl)acrylamide	0.84	Amides and imides	−0.40	0.42	O	X	Michael
110–26–9	*N, N'*-Methylenediacrylamide	−1.52	Amides and imides	−2.16	−0.19	X	X	Michael
117–80–6	2,3-Dichloro-1,4-naphthoquinone	2.65	Conjugated systems1	4.08	3.86	X	X	Michael

(*Continued*)

Table 2. Continued.

CAS	Chemical name	log P Pred.	KATE class name	log (1/LC50 [mM]) Pred.	log (1/LC50 [mM]) Meas.	Domain log P[2]	Domain C[3]	'reactive'[4]
868–63–3	2-Propenamide, *N*,*N*′-(1,2-dihydroxy-1,2-ethanediyl)bis-	−3.69	Amides and imides	−3.78	0.26	X	X	Michael
89–40–7	4-Nitrophthalimide	1.12	Nitrobenzenes	0.07	1.24	O	X	acylating
22509–74–6	*N*-Carboethoxyphthalimide	2.33	Amides and imides	0.71	2.19	O	X	acylating
78–51–3	Tri-*n*-butoxyethyl phosphate	3.00	Esters phosphate	1.96	1.28	O	*C (1)*	
88–05–1	2,4,6-Trimethylaniline	2.72	Primary amines	0.82	0.39	O	*C (1)*	
88–75–5	*o*-Nitrophenol	1.91	Amines aromatic or phenols4	0.61	0.34	O	*C (1)*	
89–64–5	4-Chloro-2-nitrophenol	2.55	Unclassified	1.00	1.20	O	*C (1)*	
91–17–8	Bicyclo[4.4.0]decane	4.20	Hydrocabons aliphatic	1.88	2.57	O	*C (1)*	
91–17–8	Bicyclo[4.4.0]decane	4.20	Neutral organics	1.86	2.57	O	*C (1)*	
95–87–4	2,5-Xylenol	2.61	Amines aromatic or phenols4	1.11	1.33	O	*C (1)*	
108–87–2	Methylcyclohexane	3.59	Hydrocabons aliphatic	1.42	1.67	O	*C (1)*	
108–87–2	Methylcyclohexane	3.59	Neutral organics	1.35	1.67	O	*C (1)*	
111–78–4	1,5-Cyclooctadiene	3.73	Hydrocabons aliphatic	1.52	0.92	O	*C (1)*	
111–78–4	1,5-Cyclooctadiene	3.73	Neutral organics	1.47	0.92	O	*C (1)*	
120–95–6	2,4-Di-*tert*-pentylphenol	6.31	Amines aromatic or phenols4	3.80	2.91	O	*C (1)*	
504–29–0	2-Aminopyridine	0.53	Amines aromatic or phenols5	−0.32	0.93	O	*C (1)*	
615–58–7	2,4-Dibromophenol	3.29	Amines aromatic or phenols4	1.61	1.84	O	*C (1)*	
634–93–5	2,4,6-Trichloroaniline	3.01	Amines aromatic or phenols3	1.59	1.57	O	*C (1)*	
716–79–0	1H-Benzimidazole, 2-phenyl-	3.00	Hydrocarbons aromatic	1.01	1.35	O	*C (1)*	
764–13–6	2,5-Dimethylhexa-2,4-diene	3.95	Hydrocarbons aliphatic	1.69	1.63	O	*C (1)*	
764–13–6	2,5-Dimethylhexa-2,4-diene	3.95	Neutral organics	1.65	1.63	O	*C (1)*	

873–32–5	*o*-Chlorobenzonitrile	2.18	Amides and imides	0.60	0.57	O	*C (1)*
948–65–2	2-Phenylindole	3.82	Hydrocarbons aromatic	1.52	2.85	O	*C (1)*
2219–82–1	6-*tert*-Butyl-*o*-cresol	3.97	Amines aromatic or Phenols4	2.10	1.58	O	*C (1)*
2243–62–1	1,5-Naphthalenediamine	1.34	Amines aromatic or Phenols3	1.23	0.97	O	*C (1)*
3295–94–1	Allyl *n*-hexyl ether	3.37	Conjugated systems2	2.37	1.46	O	*C (1)*
100–55–0	3-Hydroxymethylpyridine	−0.11	Hydrocarbons aromatic	−0.95	−0.93	X	*C (1)*
462–08–8	3-Aminopyridine	−0.11	Amines aromatic or phenols5	−0.67	1.04	X	*C (1)*
504–24–5	4-Aminopyridine	−0.11	Amines aromatic or phenols5	−0.67	1.44	X	*C (1)*
89–63–4	4-Chloro-2-nitroaniline	2.66	Amines aromatic or phenols3	1.51	1.01	O	*C (2)*
96–96–8	2-Nitro-*p*-anisidine	2.10	Amines aromatic or phenols3	1.39	0.61	O	*C (2)*
140–66–9	4-*tert*-Octylphenol	5.28	Amines aromatic or phenols4	3.05	2.76	O	*C (2)*
827–52–1	Cyclohexylbenzene	4.81	Hydrocarbons aromatic	2.15	2.13	O	*C (2)*
843–55–0	1,1-Bis (4-hydroxyphenyl)-cyclohexane	5.48	Amines aromatic or phenols4	3.19	2.17	O	*C (2)*
2100–42–7	2-Chlorohydroquinone dimethylether	2.80	Unclassified	1.19	0.79	O	*C (2)*
100–63–0	Hydrazine, phenyl-	0.79	Hydrazines (Clog P)	2.16	3.83	O	X
123–46–6	Ethanaminium, 2-hydrazino-*N,N,N*-trimethyl-2-oxo-, chloride	−5.29	Hydrazines (Clog P)	−0.37	−2.02	X	X
497–18–7	Carbonohydrazide	−3.73	Hydrazines (Clog P)	0.28	0.24	X	X
19715–19–6	3,5-Di-*tert*-butylsalicylic acid	6.06	Unclassified	3.61	1.97	X	X
90–30–2	1-(*N*-phenylamino)-naphthalene	4.47	Amines aromatic or phenols5	1.82	2.50	X	X

Note: [1]When a chemical belongs to more than one QSAR class, all the predicted data are adopted.
[2]O: In-domain of log *P*-judgement; X: out-of-domain of log *P*-judgement.
[3]*C (1)*: In-domain of *C*-judgement, defined as: (1) all substructures of a test chemical are found in reference chemicals in the class.
C (2): In-domain of *C*-judgement, defined as: (2) all substructures of a test chemical are in reference chemicals in either *Neutral organics* or the class.
X: Out-of-domain of *C*-judgement.
[4]Names of the reactive mechanistic domains are given in the text.

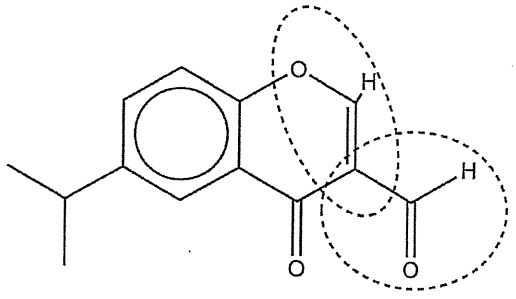

Figure 1. 3-Formyl-6-*iso*-propylchromone, with two "reactive" substructures. Dotted lines indicate Schiff base former (right) and Michael acceptor (left).

in-domains of the log *P*- and the *C(1)*-judgements were considered, in the predicted values for fish, 7 and 23 chemicals were categorised as "reactive" and "non-reactive", respectively, the corresponding figures for *Daphnia* being 6 and 25. The "reactive" chemicals in these training sets might have been chemicals that were "untrained" for (i.e. unknown in) the KATE system, because "out-of-domain" in the *C*-judgements cannot be described using known substructures of the reference dataset in the class to which the chemical belongs.

The predictivity of the KATE system, combined with the reactive domains, is summarised in Tables 4, 5 and 6. As in our previous paper [14], a criterion [47] and under- and over-estimation of predicted toxicities were adopted as measures of predictivity. In this case the *acceptable* criterion (Tables 4 and 5) was evaluated such that the common logarithm of the inverse of the estimations [mmol L^{-1}, mM] by the KATE system did not deviate from the common logarithm of the inverse of the experimental toxicities [mM] by less than a factor of 1.0.

3.1 *Fish toxicity*

Firstly, we will focus on the predicted toxicities at the fish end-point (Table 4). Of the chemicals within the "reactive" domain, 78% met the acceptable criterion, whereas 71% of the chemicals within the "reactive" domain, and the log *P*- and *C(1)*-judgements, were acceptable. The percentages of the chemicals within the "reactive" domain seemed to be independent of these judgements. Additionally, the RMSEs within the "reactive" domain *could not* be less than 1.0 after the application of the judgements (Table 6). On the other hand, RMSEs became less than 1.0 after use of the *C*-judgement (i.e. structural domains on KATE) without the inclusion of any compounds with "reactive" substructures. These findings correspond to those of a previous study that demonstrated improvement of the RMSE between prediction and measurement by applying the *C*-judgement [14]. In other words, the toxicity of a "non-reactive" chemical within these judgements is well predicted by the KATE system. The reactive domains discussed here are supplementary to the information for fish toxicity prediction by KATE.

3.2 Daphnia *toxicity*

Secondly, we shall consider the predicted toxicities at the *Daphnia* end-point (Table 5). The proportion of "reactive" chemicals meeting the acceptable criterion did not increase

Table 3. Results of KATE-based prediction, with CAS number, chemical name, toxicity of chemicals to *Daphnia* as measured and as predicted by KATE, log *P*- and *C*-judgements (KATE domains), and the "reactive" mechanistic domains (Enoch et al. [25]) for the 78 compounds in the test set.[1]

CAS	Chemical name	log P Pred.	KATE class name	log (1/EC_{50} [mM]) Pred.	log (1/EC_{50} [mM]) Meas.	Domain log P[2]	Domain C[3]	"reactive"[4]
75–34–3	1,1-Dichloroethane	1.76	Halides3	0.45	0.46	O	*C (1)*	S_N2
286–62–4	Cyclooctene oxide	2.64	Epoxides (Clog P)	1.87	0.72	O	*C (1)*	S_N2
2425–79–8	1,4-Bis (2,3-epoxypropoxy)butane	–0.15	Epoxides (Clog P)	0.52	0.96	X	*C (1)*	S_N2
535–13–7	Ethyl 2-chloropropionate	1.54	Halides1	3.8	0.66	X	X	S_N2
134–96–3	4-Hydroxy- 3,5-dimethoxybenzaldehyde	0.88	Aldehydes (Clog P)	0.75	0.64	O	*C (1)*	SB, pro-Michael
49619–58–1	3-Formyl-6-isopropylchromone	2.26	Conjugated systems2	1.39	2.08	O	X	SB, Michael
123–15–9	2-Methylvaleraldehyde	1.73	Aldehydes (Clog P)	1.2	0.82	O	*C (1)*	SB
75–07–0	Acetaldehyde	–0.17	Aldehydes (Clog P)	0.21	0.17	X	*C (1)*	SB
111–30–8	Glutaraldehyde	–0.18	Aldehydes (Clog P)	0.2	1.06	X	*C (1)*	SB
487–68–3	2,4,6-Trimethylbenzaldehyde	3.35	Aldehydes (Clog P)	2.04	1.52	O	*C (2)*	SB
90–60–8	3,5-Dichlorosalicylaldehyde	3.3	Aldehydes (Clog P)	2.01	2.13	O	X	SB
394–50–3	3-Fluoro-2-hydroxybenzaldehyde	2.21	Aldehydes (Clog P)	1.45	1.15	O	X	SB
111–18–2	*N,N,N′,N′*-Tetramethylhexamethylene-diamine	1.7	Secondary and tertiary amines	0.43	0.34	X	*C (2)*	pro-SB
6117–91–5	2-Buten-1-ol	0.63	Conjugated systems2	1.04	1.11	O	*C (1)*	pro-Michael
119–34–6	4-Amino-2-nitrophenol	0.64	Unclassified	0.42	1.85	O	*C (2)*	pro-Michael
20103–09–7	2,5-Dichloro-1,4-benzenediamine	0.9	Amines aromatic or phenols1	2.52	2.32	O	X	pro-Michael
51963–82–7	Benzenamine, 2,5-diethoxy-4-(4-morpholinyl)-	2.01	Amines aromatic or phenols1	2.61	1.17	O	X	pro-Michael
101–96–2	1,4-Benzenediamine, *N,N′*-bis (1-methylpropyl)-	3.5	Amines aromatic or phenols1	2.74	2.61	X	X	pro-Michael
40220–08–4	Tris (2-hydroxyethyl)isocyanuric acid acrylate	3.75	Amides and imides	1.38	0.69	O	X	Michael, acylating
40220–08–4	Tris (2-hydroxyethyl)isocyanuric acid acrylate	3.75	Acrylates	1.41	0.69	X	X	Michael, acylating
100–43–6	4-Vinylpyridine	1.71	Hydrocarbons aromatic	0.62	1.94	O	*C (1)*	Michael
1335–46–2	Methylionone	4.84	Conjugated systems2	1.94	1.82	X	*C (2)*	Michael
98–81–7	α-Bromostyrene	3.29	Unclassified	1.84	2.74	O	X	Michael
117–80–6	2,3-Dichloro-1,4-naphthoquinone	2.65	Conjugated systems1 (Clog P)	3.06	4.13	O	X	Michael

(*Continued*)